Electromagnetic generation of ultrasound in ferromagnets

V. D. Buchel'nikov and A. N. Vasil'ev

Moscow State University

(Submitted 18 October 1991)
Usp. Fiz. Nauk. **162**, 89–128 (March 1992)

This review discusses the principal physical mechanisms responsible for direct electromagnetic-acoustic conversion in ferromagnets. It is shown that in a wide range of frequency, magnetic field, and temperature ultrasound is generated via the inductive and magnetoelastic interactions. In the latter mechanism features are observed that are due to the displacement of domain walls and spin flip, and are also observed at various phase transitions. A detailed comparison of the theory of electromagnetic excitation of ultrasound with experimental data obtained for 3d and 4f magnets also showed that this phenomenon can be used as a precise method of constructing magnetic phase diagrams of magnets and determining their homogeneous and inhomogeneous exchange interaction constants, and the magnetic anisotropy and magnetostriction constants.

INTRODUCTION

The incidence of an electromagnetic wave on the surface of a conducting solid is accompanied by the excitation of ultrasonic oscillations. The variety of the experimental and theoretical methods used to study this phenomenon constitute now a separate field in solid state physics at the interface between traditional spectroscopy and radiospectroscopy. The concept of electromagnetic generation of ultrasound was formulated in the 1960s in the work of Kontorovich *et al.*,[1–3] and Kaganov and Fiks,[4–6] where the conversion of electromagnetic and acoustic waves in normal metals was considered. In these media the source of elastic waves is the force exerted on lattice by the electron subsystem.

Electromagnetic-acoustic conversion (EAC) takes place both in the linear regime, where the frequency of elastic oscillations coincides with frequency of the incident wave, and in the nonlinear regime, when the frequency of ultrasound is a multiple of the frequency of the electromagnetic wave. Below we will deal only with the linear mechanisms of EAC.

An electromagnetic wave incident on a metal surface is reflected almost completely, with only a small part of its energy penetrating the skin layer and dissipating in the metal as Joule heat. In the absence of a static magnetic field the excitation of ultrasound occurs to an experimentally observable extent only under conditions of the anomalous skin-effect, where the mean free path of electrons exceeds skin depth. In this case the direct action of the electric field of the wave on the ions in skin layer is not compensated locally by their collisions with electrons. The latter transfer their excess momentum to the lattice in a surface layer with a thickness of the order of the election mean free path. A detailed study of this so-called deformation mechanism was carried out in the original works of Gantmacher and Dolgopolov,[7,8] Kaner *et al.*,[9,10] Gaerttner, Wallace and Maxfield,[11] Chimenti, Kukkonen and Maxfield,[12] Overhauser *et al.*,[13–15] Rodriguez *et al.*,[16–21] and also in the review by Rodriguez, Kartheuser and Ram Mohan.[22]

To observe the electromagnetic-acoustic conversion under conditions of the normal skin effect it is necessary to apply to metal both an ac magnetic field and a static magnetic field $\mathbf{H}_0$.

Here the electrons are acted on by the Lorentz force, whose direction is determined by the orientation of the field $\mathbf{H}_0$ relative to the surface of the metal. This so-called inductive mechanism of conversion was investigated in the works of Gaidukov and Perov,[23–25] Kravchenko,[26] Vlasov *et al.*,[27–29] Quinn,[30–32] Alig,[33] Southgate,[34] Dobbs *et al.*,[35–38] the reviews on this mechanism of EAC are given by Wallace,[39] Dobbs,[40] and Vasil'ev and Gaidukov.[41]

Besides the deformation and inductive mechanisms of EAC the generation of ultrasound occurs via universal conversion mechanisms that take place in all conducting media, i.e., via the thermoelastic[42] and inertial (Stewart-Tolmen effect)[43] interactions. These mechanisms of EAC have not been experimentally investigated yet, and are not considered here.

In addition to the induction interaction, modified by the presence of a magnetic subsystem, magnetically ordered media also exhibit EAC mechanisms that are specific to magnets. It is well known that the magnets change their shape and dimensions under action of a magnetic field.[44] Both the isotropic, and the anisotropic magnetostrictions are due to the interaction of this field with the system of atomic magnetic moments, which results, through the magnetoelastic interaction constants, in a deformation of the solid. The linear excitation of ultrasound through magnetostriction occurs only in single-domain magnets. In polydomain magnets in an ac magnetic field elastic deformations are induced at double the frequency of the perturbation. It is clear that with the use of magnetostriction for generating elastic waves in the linear regime in polydomain magnets it is necessary to use a static magnetizing field.

In fact, any processes that magnetize the material have an effect on the processes of electromagnetic-acoustic conversion. For example, with an electromagnetic field incident on the surface of a magnet ultrasound is excited via the displacement of the domain walls and via the rotation of the magnetization in the domains. The phenomenon of EAC occurs in different ways in samples with a regular or a nonregular domain structure. Moreover, the magnetic ordering such as takes place at the Curie point of a ferromagnet, or the change in the type of magnetic ordering such as occurs, for example, in the transition from the antiferromagnetic phase to the ferromagnetic phase, is also accompanied by sharp peaks in the efficiency of the transformation.

The electromagnetic generation of ultrasound in mag-

0038-5670/92/030192-20$03.00

netically ordered materials was investigated by Budenkov *et al.*,[45–47] Gitis,[48] Drobotko and Nabereshnykh,[49,50] Ilyasov and Komarov,[51,52] Povey *et al.*,[53–55] Privorotsky *et al.*,[56] Alexandrakis and Devine,[57] Gordon,[58] Hanabusa *et al.*,[59] Luthi *et al.*,[60] and Andrianov *et al.*[61–67]

An analysis of the features of the magnetoacoustic mechanism of EAC is contained in reviews by Frost,[71] Budenkov and Gurevich,[72] as well as in the monographs of Shkarlet[73] and Komarov.[74] References 71–74 provide a large bibliography of articles dealing with the use of electromagnetic excitation of ultrasound in a variety of svstems of nondestructive testing and diagnostics.

Both in practical application and in scientific research there are qualitatively different approaches to EAC investigations in normal and magnetically ordered materials. The generation of ultrasound in normal metals by the Lorentz force is efficient only when the wavelength of the ultrasound exceeds the skin depth; this means that a "smeared" force could not excite short acoustic waves. This condition is fulfilled in pure metals at frequencies ω less than 10^{10} sec^{-1}, which determines the frequency range of EAC study. Just the opposite situation is obtained when magnetostriction is used for ultrasound generation. Here the entire volume of the magnet participates in the process. In this case the magnetostrictive material should be prepared as a fine powder with a grain size less than skin depth.

The subject of this paper concerns the waves in magnetostrictive materials, i.e., the investigation of electromagnetic generation of ultrasound in conducting magnets. The EAC studies in magnets are based on system of equations describing coupled oscillations of the electromagnetic, elastic and spin subsystems in a metal. The spectra of these oscillations in cubic and uniaxial ferromagnets have been studied in the works of Povey, Meredith and Dobbs,[53] and of Baryachtar, Grishin and Drobotko.[75] The dispersion equations for coupled oscillations in hexagonal ferromagnets have been derived by Andrianov *et al.*[64,66] The calculation of the efficiency of ultrasound generation in magnets by electromagnetic waves is of interest both for the study of the interaction between different types of elementary excitations in solids and for the purpose of obtaining new information about their magnetic properties, i.e., to reconstruct their magnetic phase diagrams, or to determine the exchange constants and the parameters of magnetic anisotropy and magnetostriction.

1. SPECTRUM OF NATURAL OSCILLATIONS OF A FERROMAGNETIC METAL

The spectrum of elementary excitations of a ferromagnet includes electromagnetic, spin, and elastic oscillations. Only in the first approximation can these be considered as independent. In general, and in EAC considerations in particular, it is necessary to take into account their interactions. Because of these interactions, the normal modes of oscillations are coupled waves. To avoid misunderstanding, we stipulate here that we do not consider weakly damped electromagnetic modes, i.e., helicons, dopplerons, etc., which can propagate only in a very pure metal at low temperature in the presence of a static magnetic field.

1.1. System of equations of interacting electromagnetic, spin, and elastic waves in magnets

The study of the excitation of ultrasound by an electromagnetic wave incident on the surface of a magnetic metal assumes the solution of the coupled system of equations describing the propagation, as well as the interaction of electromagnetic, spin, and elastic oscillations. This system includes the elasticity equation, the Maxwell equations, and the Landau–Lifshitz equation for the magnetization:

$$\rho_M \ddot{\mathbf{U}} = \mathbf{f}. \tag{1}$$

$$\mathrm{rot}\,\mathbf{H} = \frac{4\pi}{c}\mathbf{j}, \tag{2}$$

$$\mathrm{rot}\,\mathbf{E} = -\frac{1}{c}\frac{\partial \mathbf{B}}{\partial t}, \tag{3}$$

$$\dot{\mathbf{M}} = g[\mathbf{M}, \mathbf{H}^{\mathrm{eff}}] + \mathbf{R}. \tag{4}$$

Here ρ_M is the density of the material, $\mathbf{U}$ is the displacement, $\dot{\mathbf{U}} = \partial \mathbf{U}/\partial t$, $\mathbf{f}$ is the density of force, acting on an elementary volume of the magnet, $\mathbf{H}$ and $\mathbf{E}$ are the magnetic and electric fields, respectively, $\mathbf{B}$ is the magnetic induction, c is the velocity of light, $\mathbf{j}$ is the current density, $\mathbf{M}$ is the magnetization, g is the gyromagnetic ratio, $\mathbf{H}^{\mathrm{eff}} = -\delta F/\delta \mathbf{M}$ is the effective magnetic field, F is the free energy density of the magnet, and R is the relaxation term in the magnetic subsystem.

The components of the volume force density vector are $f_i = \partial \sigma_{ik}/\partial x_k$, where the mechanical stress tensor can be written as:[76]

$$\sigma_{ik} = \sigma_{ik}^{(e)} + \sigma_{ik}^{(me)} + \sigma_{ik}^{(em)} + \sigma'_{ik}. \tag{5}$$

Here the elastic and magnetoelastic stress tensor are, respectively

$$\sigma_{ik}^{(e,me)} = \frac{\partial F_{e,me}}{\partial U_{ik}}.$$

The electromagnetic stress tensor is

$$\sigma_{ik}^{(em)} = \frac{1}{4\pi}\left(H_i B_k - \frac{1}{2}H^2\delta_{ik}\right).$$

The term that describes the attenuation in the elastic subsystem is

$$\sigma'_{ik} = \frac{1}{2}\eta_{iklm}\dot{U}_{lm},$$

where η_{iklm} is the viscosity tensor, F_e is the free energy density in the elastic subsystem, F_{me} is the density of magnetoelastic energy (magnetostriction energy), and U_{ik} is the strain tensor.

The current density in the laboratory reference frame can be determined with the use of equation

$$E_i = \rho_{ik} j_k + R^{\mathrm{B}}_{ikm} B_m j_k + R^{\mathrm{M}}_{ikm} M_m j_k - ([\dot{\mathbf{U}}, \mathbf{B}]_i/c), \tag{6}$$

where ρ_{ik} is the resistivity tensor and R^{B} and R^{M} are the tensors of normal and anomalous Hall effects, respectively.

The Maxwell equations should be completed with

$$\mathrm{div}\,\mathbf{B} = 0. \tag{7}$$

The relaxation term in Eq. (4) can be written as

$$\mathbf{R} = -\frac{1}{\tau_2}\mathbf{H}^{\text{eff}} - \frac{1}{\tau_1 \mathbf{M}^2}[\mathbf{M}[\mathbf{M}, \mathbf{H}^{\text{eff}}]], \tag{8}$$

where $\tau_{1,2}$ are the transverse and longitudinal relaxation times.

The free energy density of a magnet is

$$F = \frac{1}{2}a\mathbf{M}^2 + \frac{1}{4}b\mathbf{M}^4 + \alpha_{ik}\frac{\partial \mathbf{M}}{\partial x_i}\frac{\partial \mathbf{M}}{\partial x_k} + F_a + \frac{1}{2}\gamma_{ik}\mathbf{M}^2 U_{ik} + \gamma_{ijkl}M_i M_j U_{kl} + C_{ijkl}U_{ij}U_{kl} - \mathbf{M}(\mathbf{H}_0 + \mathbf{h}), \tag{9}$$

where a and b are the homogeneous exchange constants, α, γ, and C are the inhomogeneous exchange, magnetostriction, and elasticity tensors, respectively. The first three terms in expression (9) describe the homogeneous and inhomogeneous exchange energies and the fourth term describes the magnetization anisotropy energy. The fifth and sixth terms in (9) describe the energy of isotropic (exchange) and anisotropic magnetostriction. The seventh term is the elastic energy, and the last term is the Zeeman energy, which describes the interaction of the magnetization with a static magnetic field $\mathbf{H}_0$ and an ac field $\mathbf{h} \sim \mathbf{h}_0 \exp(-i\omega t)$, where ω is the frequency of the incident electromagnetic wave.

When investigating EAC in isotropic magnets, polycrystalline materials, and in ferromagnets with a nonregular domain structure one can use, instead of the Landau–Lifshitz equation for the magnetization (4), the relation

$$\mathbf{M} = \chi \mathbf{H}, \tag{10}$$

where χ is the magnetic susceptibility tensor. Equation (10) connects the static and the ac magnetic fields with the magnetizations. Theoretically, the tensor χ can be obtained from the solution of system of equations (1)–(4) for the separate crystallite (or domain) with subsequent averaging over the entire crystal (or domain), but we shall use Eq. (10), assuming that χ can be determined from independent measurements. Besides, for the isotropic magnets, polycrystalline materials, and ferromagnets with a nonregular domain structure we can use the following expression for the free energy

$$F = \frac{1}{2}A\mathbf{M}^2 + \frac{1}{4}B\mathbf{M}^4 + \frac{1}{2}\gamma\mathbf{M}^2 U_{ii} + \frac{1}{2}\lambda_1 U_{ii}^2 + \lambda_2 U_{ik}^2, \tag{11}$$

where A and B are the homogeneous exchange constants (A and B also include the anisotropy constants because of the averaging (9) over the crystallites), γ is the volume magnetostriction constant (it contains both the exchange and anisotropy constants, which also come in in the averaging), and λ_1 and λ_2 are the Lame coefficients.

1.2. Boundary conditions

The system of equations (1)–(4) should be augmented with the boundary conditions for the vectors **E**, **H**, and **B**, as well as for the stress tensor σ_{ik} and magnetization **M**. In the laboratory reference frame the continuity of the normal components of the magnetic induction and of the tangential components of the electric and magnetic fields at the surface of the magnet can be written as

$$B_n^{(i)} = B_n^{(e)},$$
$$[\mathbf{n}, (\mathbf{E}^{(i)} - \mathbf{E}^{(e)})] = \frac{1}{c}\dot{U}_n(\mathbf{B}^{(i)} - \mathbf{B}^{(e)}), \tag{12a}$$
$$[\mathbf{n}, (\mathbf{H}^{(i)} - \mathbf{H}^{(e)})] = 0.$$

For the magnet free surface the condition of continuity of the stress tensor is

$$\sigma_{ik}^{(i)} n_k = \sigma_{ik}^{(e)} n_k, \tag{12b}$$

where the indices i and e serve to denote the variables interior and exterior to the material, respectively, and **n** is the normal to the surface.

The boundary condition for the magnetization of a material is

$$n_k \frac{\partial F}{\partial(\partial \mathbf{M}/\partial x_k)} = 0. \tag{12c}$$

1.3. Dispersion relation and spectra of coupled oscillations

The system of equations (1)–(4) makes it possible to calculate the spectra of interacting coupled electromagnetic, spin, and elastic waves in unbounded magnets. Calculations of this sort have been done for cubic,[53] for uniaxial elastically and magnetoelastically isotropic,[75] and for hexagonal ferromagnets.[64,66]

The dispersion equation for coupled oscillations propagating along the sixfold c axis in a hexagonal ferromagnet is

$$(q^2 - k_S^2)(q^2 - k_E^2)(q^2 - k_A^2) - (4\pi/\alpha)k_E^2(q^2 - k_A^2) - (\xi/\alpha)k_A^2(q^2 - k_E^2) - \varepsilon k_E^2 q^2(q^2 - k_S^2) - 4(\pi\varepsilon\xi/\alpha^2)^{1/2}k_E^2 q^2 = 0, \tag{13}$$

where

$$k_S^2 = -(\omega_0 \mp \omega)/gM\alpha, \quad k_E^2 = 2i/\delta^2, \quad k_A^2 = \omega^2/S_4^2 \tag{14}$$

are the squares of the wavenumbers of the noninteracting oscillations, α is the inhomogeneous exchange constant along the sixfold axis, $\xi = \gamma^2 M^2/\rho_M S_4^2$ is the magnetoelastic interaction parameter, $\varepsilon = H_0^2/4\pi\rho_M S_4^2$ is the electromagnetic-acoustic interaction parameter, the value 4π serves as the parameter of the electromagnetic-spin-interaction, S_4 is the velocity of transverse ultrasound, $\delta = (c^2\rho/2\pi\omega)^{1/2}$ is the skin depth in a nonmagnetic metal, ρ is the resistivity, $\omega_0 = g(H_0 + K/M)$ is the frequency of homogeneous spin oscillations, K is the sum of the constants of uniaxial magnetic anisotropy renormalized by magnetostriction and the static magnetic field is $\mathbf{H}_0 \| \mathbf{c}$.

The dispersion equation (13) is written under the assumption that in the absence of a static magnetic field the magnetization **M** is tilted from the **c** axis. When the magnetic field is applied the spins are reoriented in this direction. In a field $H_0 = -K/M$ a second-order orientational phase transition occurs.[77] The spectra of bound electromagnetic, spin, and elastic waves in the + polarization, propagating along the sixfold symmetry axis in a hexagonal ferromagnetic metal far from the orientational phase transition, are shown in Figs. 1 and 2. The dashed lines show the noninteracting branches, and the solid lines the branches of coupled

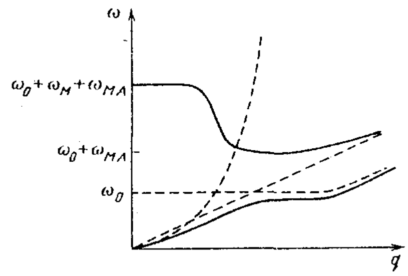

FIG. 1. Spectrum of coupled oscillations of a ferromagnetic metal far from the spin-flip transition. ω_M and ω_{MA} are the gaps in spin wave spectrum, caused by their interaction with electromagnetic and elastic waves.

oscillations. We emphasize the arbitrary way in which the imaging of the parabolic branches of the electromagnetic waves is done in these figures. They contain equal real and imaginary parts and do not propagate outside the skin layer. In the regions where the noninteracting elastic waves and spin waves intersect with the electromagnetic waves the damping of the coupled waves increases sharply. They also essentially do not get out of the skin layer. For small wave vectors the gap in the spectrum of quasispin oscillations is determined by the magnetostatic and magnetoelastic contributions. Beyond the intersection points of the noninteracting spin and electromagnetic waves the gap is determined by only the magnetoelastic contribution.

1.4. Excitation of elastic modes and main approximations

The system of equations (1)–(4) with the boundary conditions (12), besides allowing us to calculate the spectra of eigenoscillations of conducting ferromagnets also allows us to determine the efficiency of excitation of the different spectral modes by external perturbations. The driving force in the elasticity equation, according to Eq. (5), is due to the various interactions in magnetically ordered materials. The term $\partial\sigma_{ik}^{(me)}/\partial x_k$ is responsible for the magnetoelastic mechanism of the generation of ultrasound, while the term $\partial\sigma_{ik}^{(em)}/\partial x_k$ embodies the inductive mechanism.

Let us enumerate the main assumptions used to solve the problem of electromagnetic generation of ultrasound. First, we consider only highly conductive ferromagnets. We assume also, that the conductivity of a metal is isotropic and the conditions of a normal skin effect are fulfilled. The off-diagonal components of the conductivity, which are due to the Hall effect, are neglected. The elastic and magnetoelastic properties of a substance are assumed either isotropic (Secs. 2 and 3), or of the hexagonal symmetry (Secs. 4 and 5). The latter materials are the rare-earth metals. In the expression

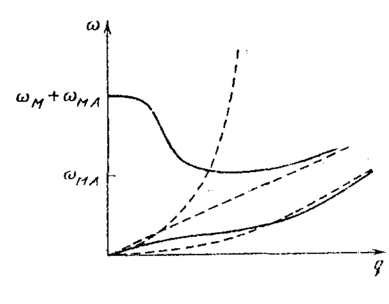

FIG. 2. Spectrum of coupled oscillations of ferromagnetic metal at the spin-flip transition $\omega_0 = 0$.

for the free energy (9) we neglect the inhomogeneous exchange term. In this case there is no dispersion in the spectrum of either the quasispin, or the quasiacoustic waves. Moreover, it is not necessary to consider the boundary condition for the magnetization, Eq. (12c). These assumptions which allow us to neglect the inhomogeneous exchange term in Eq. (9), as well as the influence of this term on the generation of transverse ultrasound, are considered in Sec. 5.

2. ELECTROMAGNETIC EXCITATION OF ULTRASOUND IN ISOTROPIC FERROMAGNETS

Let us first consider the very simple case of electromagnetic-acoustic conversion in a metal with isotropic elastic and magnetoelastic properties. The sources of excitation in this case are the inductive and magnetoelastic interactions. In the latter we take into account only the isotropic exchange magnetostriction. For the sake of clarity we consider the situation, where the static magnetic field $\mathbf{H}_0$ is oriented parallel to the plane of metal surface and is parallel to the ac magnetic field $\mathbf{h}$:($\mathbf{H}_0\|\mathbf{h}\|\mathbf{x}$), while the wavevector of the ultrasound $\mathbf{k}$ is oriented along the normal $\mathbf{n}$ to the surface ($\mathbf{k}\|\mathbf{n}\|\mathbf{z}$). This is the geometry in which longitudinal ultrasonic waves are excited.

The system of equations describing the propagation of electromagnetic and ultrasonic waves in metal can be written as

$$\left[k_A^2(1-\xi)^{-1}+\frac{\partial^2}{\partial z^2}\right]U-\frac{1}{4\pi\rho_M\tilde{S}^2}(H_0+4\pi\gamma M\chi)\frac{\partial h}{\partial z}=0,$$
$$\left(\mu k_E^2+\frac{\partial^2}{\partial z^2}\right)h+k_E^2(\mu H_0+4\pi\gamma M\chi)\frac{\partial U}{\partial z}=0, \qquad (15)$$

where k_E and k_A are given by Eq. (14), and $\tilde{S}=S(1-\xi)^{-1/2}$ is the velocity of longitudinal ultrasound renormalized by the magnetoelastic interaction, $S^2=(\lambda_1+2\lambda_2)/\rho_M$.

The dispersion equation, which determines the eigenwavevectors q_1 and q_2 is

$$[q^2-k_A^2(1-\xi)^{-1}](q^2-\mu k_E^2)$$
$$=q^2\frac{k_E^2}{4\pi\rho_M\tilde{S}^2}(H_0+4\pi\gamma M\chi)(\mu H_0+4\pi\gamma M\chi). \qquad (16)$$

The general solution of the system of equations (15) can be written as a sum of elastic waves

$$U(z)=U_1\exp(iq_1z)+U_2\exp(iq_2z).$$

One of these, with amplitude U_1, is attenuated within the skin layer, while the other wave with amplitude U_2 propagates into the metal.

The boundary conditions in the problem of ultrasound generation in magnets by electromagnetic waves are

$$q_1U_1+q_2U_2+\frac{i\gamma M\chi}{\rho_M\tilde{S}^2}(h_1+h_2)=0,$$
$$h_1+h_2=h_0+h_R, \qquad (17)$$
$$\frac{c\rho}{4\pi}(q_1h_1+q_2h_2)+\frac{i\omega}{c}H_0(U_1+U_2)=-h_0+h_R$$

Here h_1 and h_2 are the amplitudes of electromagnetic waves propagating in metal h_0 is the amplitude of the incident wave, and h_R is the amplitude of the reflected wave. As was stressed above, the possibility of separating the different terms in the stress tensor (5) which have different physical origins makes it possible to separate the mechanisms responsible for the generation of ultrasound in magnets.

2.1. Inductive interaction

Among the numerous mechanisms of direct conversion of electromagnetic and acoustic waves in metals the inductive interaction is of particular importance. This very simple and at the same time most powerful and universal mechanism of conversion is in essence the Lorentz interaction between the alternating current induced by the electromagnetic wave in the skin layer of a metal and the static magnetic field. Because of the Lorentz force, longitudinal and transverse waves, as well as various types of surface waves are excited with comparable efficiency. This mechanism of EAC works in a wide range of frequency, magnetic field, and temperature. It should be noted, that the details of the electronic properties of a metal have little effect on the conversion processes. The role of the Lorentz force is to create an alternating pressure imposed on the lattice by the electron gas.

To study the inductive mechanism of conversion in ferromagnets it is sufficient to take into account the magnetic subsystem in the metal by introducing an effective magnetic susceptibility and correspondingly renormalizing the penetration depth of the electromagnetic field in the metal. One can exclude from consideration the magnetoelastic interaction by setting formally $\gamma = 0$. In this case, the roots of the dispersion equation (16) are

$$q_1^2 = \mu k_E^2 \times \begin{cases} 1, & \beta \gg 1, \\ 1+\varepsilon, & \beta \ll 1, \end{cases} \tag{18a}$$

$$q_2^2 = k_A^2 \times \begin{cases} 1, & \beta \gg 1, \\ (1+\varepsilon)^{-1}, & \beta \ll 1, \end{cases} \tag{18b}$$

where $\beta = (k_A/|k_E|)^2$ is the parameter that describes the spatial distribution of the driving force. In the radio frequency range (i.e., $\omega \leqslant 10^{10}$ s^{-1}) the case $\beta \ll 1$ corresponds to good conductors, while the case $\beta \gg 1$ corresponds to poor conductors. In experimental practice ($H_0 \leqslant 10^5$ Oe) the parameter of the electromagnetic-acoustic interaction is $\varepsilon < 1$.

The first root describes a quasielectromagnetic wave that is damped in the interior of the metal, and the second is the quasiacoustic longitudinal wave of amplitude

$$|U_2| = \frac{H_0 h_0}{2\pi\rho_M \tilde{S}\omega}(1+\beta^2)^{-1/2}. \tag{19}$$

Here the renormalization of the velocity of ultrasound is due to the electromagnetic-acoustic interaction

$$\tilde{S} = S \times \begin{cases} 1, & \beta \gg 1, \\ (1+\varepsilon)^{1/2}, & \beta \ll 1. \end{cases} \tag{20}$$

Equation (20) describes the observable phenomenon, i.e., the change in the velocity of ultrasound in a magnetic field.[78,79]

The processes of electromagnetic-acoustic conversion can be characterized both by the amplitude of excitation (19), and by the dimensionless conversion efficiency, which can be introduced as the ratio of the acoustic energy flux $W_A = \rho_M U^2\omega^2\tilde{S}/2$ to the electromagnetic energy flux in the incident wave $W_E = ch_0^2/8\pi$:

$$\eta = \frac{H_0^2}{\pi\rho_M c\tilde{S}(1+\beta^2)} = 4\frac{\tilde{S}}{c}\frac{\varepsilon}{1+\beta^2}. \tag{21}$$

If the penetration depth of the electromagnetic wave is small compared to the wavelength of excited ultrasound ($\beta \ll 1$) the efficiency of the inductive conversion mechanism is essentially the same as the efficiency of this interaction in a nonmagnetic metal. At higher frequencies, however, when $\beta \gg 1$ all the processes occurring in the magnetic subsystem influence the conversion efficiency. In this case, the efficiency of the inductive mechanism in ferromagnets in proportional, not to the intensity of the external magnetic field, but to the magnetic induction in the metal, $B_0 = \mu H_0$.

When the magnetic field H_0 is normal to the metal surface the transverse ultrasound is excited via the inductive interaction. The amplitude of generation and the EAC efficiency are given by Eqs. (19) and (21), where S must be taken to mean the velocity of transverse ultrasound.

2.2. Magnetoelastic interaction

To analyze the generation of longitudinal ultrasound in magnets due to the magnetoelastic interaction it is necessary formally to set H_0 equal to zero in Eqs. (15)–(17). This is equivalent to neglecting the inductive conversion mechanism. In this case the roots of dispersion equation (16) are

$$q_1^2 = \mu k_E^2 \times \begin{cases} 1, & \beta \gg 1, \\ (\mu-\xi)/\mu(1-\xi), & \beta \ll 1, \end{cases} \tag{22a}$$

$$q_2^2 = (1-\xi)^{-1} k_A^2 \times \begin{cases} 1, & \beta \gg 1, \\ \mu(1-\xi)/(\mu-\xi), & \beta \ll 1. \end{cases} \tag{22b}$$

The amplitude of the propagating elastic mode in the metal is

$$|U_2| = \frac{c^2}{S^2}\frac{\gamma\chi\rho M h_0}{4\pi\rho_M S(1+\beta^2)^{1/2}} \times \begin{cases} \mu^{-1}(1-\xi)^{-3/2}, & \beta \gg 1, \\ \mu^{1/2}(\mu-\xi)^{-3/2}, & \beta \ll 1. \end{cases} \tag{23}$$

and the efficiency of the magnetoelastic generation of longitudinal ultrasound is

$$\eta = \frac{c^3}{S^3}\frac{(\gamma\chi M\rho\omega)^2(1-\xi)^{1/2}}{4\pi\rho_M S^2(1+\beta^2)} \times \begin{cases} \mu^{-2}(1-\xi)^{-3}, & \beta \gg 1, \\ \mu(\mu-\xi)^{-3}, & \beta \ll 1. \end{cases} \tag{24}$$

It can be seen that the most efficient magnetoelastic generation occurs in the region of the transition from the paramagnetic into the ferromagnetic state. Formally, the peak in the ultrasound generation in this region is due to the nonmonotonic temperature variation of the product of the magnetization M and the magnetic susceptibility χ. Physically, the sharp increase in the efficiency of EAC at the Curie temperature is due to the fact that the liability of the spin subsystem increases at the phase transition. If the magnetostriction is not equal to zero the modulation of the magnetization of the magnet by the field of electromagnetic wave results in intense excitation of ultrasound. The transverse elastic waves are not excited by isotropic exchange magnetostriction.

2.3. Comparison of the efficiencies of the inductive and magnetoelastic mechanisms of EAC

Using the expressions $M = \chi H$ and $\rho = 1/\sigma$ and assuming that the parameters of the magnetoelastic, ξ, and electromagnetic-acoustic, ε, interactions are small compared to unity, one can write the relation between magnetoelastic and inductive conversion mechanisms as

$$\frac{\eta^{\mathrm{ME}}}{\eta^{\mathrm{EM}}} = \left(\frac{c}{S}\right)^4 \left(\frac{\gamma\chi^2}{\mu}\right)^2 \left(\frac{\omega}{2\sigma}\right)^2 = \left(\frac{\beta\gamma\chi^2}{\mu}\right)^2. \tag{25}$$

In particular, it follows from this expression that with all the parameters fixed the role of the inductive interaction increases with the metal conductivity. A comparison of the efficiency of the inductive and magnetoelastic mechanisms of EAC, obtained by simultaneous measurements of conductivity and magnetic susceptibility, makes it possible to determine the constants of magnetoelastic interaction.

2.4. Experimental methods

It is convenient to analyze the expressions obtained Eqs. (21), (24), and (25) on the basis of experimental data. Before discussing these data, however, let us consider the principles of the experimental approach. As follows from the above analysis, to obtain noncontact excitation of ultrasound in a magnet one should place it into both a static and an ac magnetic field. In the case of longitudinal ultrasound generation the $\mathbf{H}_0$ vector should be applied parallel to the metal surface, as shown in Fig. 3. If $\mathbf{H}_0$ is normal to the metal surface, as shown in Fig. 4, then transverse ultrasound is generated. The electric field is produced by inductive coils, ordinarily located about 10^{-1} cm from the surface. It is the near-surface layer of the magnet that converts electromagnetic and acoustic energy in EAC problems. By forming the various configurations of the magnetic field at the metal surface one can excite not only volume elastic waves that propagate at any angle to the surface, but also various types of surface elastic waves.

At present, two qualitatively different approaches are used most frequently; i.e. the pulse-echo technique and the standing-wave technique. Let us consider the former, taking for example the method[61] used to study electromagnetic generation of ultrasound in rare-earth ferromagnets.

The specimen was placed in solenoidal induction coil to which radiofrequency pulses of voltage about 1 kV were applied, of 1 μsec duration, and with a carrier frequency 10 MHz. These pulses, by some conversion mechanism, excited a sequence of damping acoustic echo signals. The inverse duty cycle of the driving rf pulses was chosen so that all of the sequence could fit between the pulses. The coil with the sample was placed in a static magnetic field in a constant temperature region with a controllable temperature. Ultrasonic pulses at the frequency of the incident electromagnetic wave were generated in the two opposite faces of the sample and propagated along the normal to them and, on reaching the opposite surface of the specimen, were detected by the same coil through inverse electromagnetic-acoustic conversion. The sequence of the echo signals, with intervals $t = d/S$ between them (where d is the thickness of the sample), were first fed to a wide-band amplifier, then to a pulse-height analyzer and then to a recorder. The amplitudes of some, usually the third or fourth echo-signal, were recorded in this manner. By varying the magnetic field strength or the temperature, the field and temperature dependences of the efficiency of EAC were recorded. The measured signal in such a study is $A \sim \eta \exp(-N\Gamma d)$, where Γ is the ultrasound attenuation and N is the echo-signal number. The attenuation of ultrasound could be determined in the same experiment by the decay rate of the echo signals, and the velocity of ultrasound could be determined by the transit time of the echo-signals.

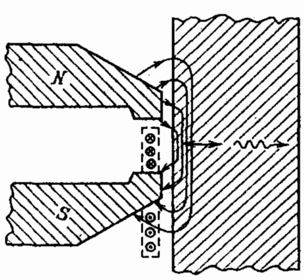

FIG. 3. Standard arrangement of the sources of static and ac magnetic fields with respect to the metal surface in the case of longitudinal ultrasound excitation.

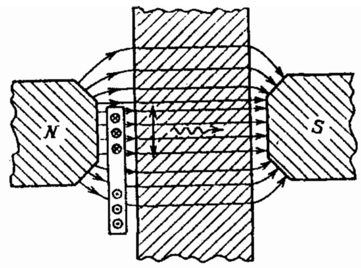

FIG. 4. Standard arrangement of the sources of static and ac magnetic fields with respect to the metal surface in the case of transverse ultrasound excitation.

The second widely used method of the EAC study is the investigation of the resonant peaks of the plate surface impedance, which are observed at the frequencies of the standing acoustic waves in the sample.[80] In such an arrangement the specimen is placed in two mutually parallel solenoidal induction coils. One of them is used to excite ultrasound and the other to detect it. The generation of ultrasound occurs over a broad frequency range, but at the resonant frequencies $\omega_n = \pi n S/d$, where $n = 1, 3,..$, the amplitude of the excited elastic waves sharply increases. Of course, the ultrasound is not detected directly, but by recording the amplitude of the electromagnetic wave emitted from the metal surface. In this approach the amplitudes of the acoustic standing wave resonances are proportional to the conversion efficiency η and inversely proportional to the attenuation Γ of ultrasound. The attenuation could be determined by the halfwidth of resonance line, and the velocity of ultrasound by the resonant frequency.

The analysis of the electromagnetic generation of ultrasound in isotropic magnets can be illustrated by experimental studies of electromagnetic-acoustic conversion in ferromagnetic 3d-metals. The field dependence of the amplitude of excitation of the surface acoustic waves in polycrystalline iron[68] obtained by the pulse-echo technique is shown in Fig. 5. It is evident that in weak magnetic fields the magnetoelastic mechanism of excitation, whose characteristic feature is a nonmonotonic field dependence, is dominant. In accordance with Eq. (23), this behavior is explained by the nonmonotonic variation with the magnetic field of the magnetic susceptibility χ and magnetostriction γ of the magnet. The value of χ is small in both weak and strong magnetic fields and reaches its maximum value at intermediate fields, where the change of slope of the magnetization curve is most pronounced.

The magnetostriction of iron varies nonmonotonically with the magnetic field, going to zero for a certain field value H_0. The presence of two peaks in weak fields is related to this behavior. With a further increase in the magnetic field the inductive interaction (19) begins to play the main role, so that the amplitude of ultrasound generation depends linearly on the magnetic field.

The field dependences of the EAC efficiency in nickel and its alloys,[58] measured by the standing wave technique, are shown in Fig. 6. It can be seen that in strong magnetic fields the inductive interaction Eq. (19) dominates. The degree to which the magnetoelastic interaction Eq. (24) shows up in weak fields depends on the value of the magnetostriction, which is the largest in Inconel. The temperature dependences of the efficiency of excitation of transverse and longitudinal ultrasound in iron[81] are shown in Fig. 7. When the metal transforms from the ferromagnetic to the paramagnetic state the generation efficiency of the transverse waves decreases sharply and there is a peak in the generation of longitudinal waves. This latter result is in agreement with formula (24), from which it follows that near the Curie temperature longitudinal ultrasound is generated most intensely. Analogous curves for polycrystalline terbium in a magnetic field greater than the threshold for the existence of the antiferromagnetic phase[61] are shown in Fig. 8. In fields below the threshold field peaks are observed in the generation efficiency in 4f magnets[62] in the transition from the paramagnetic phase into the antiferromagnetic phase and from the antiferromagnetic phase to the ferromagnetic phase. In each of these transitions there is an increase in the magnetic susceptibility, and this gives rise to the observed behavior.

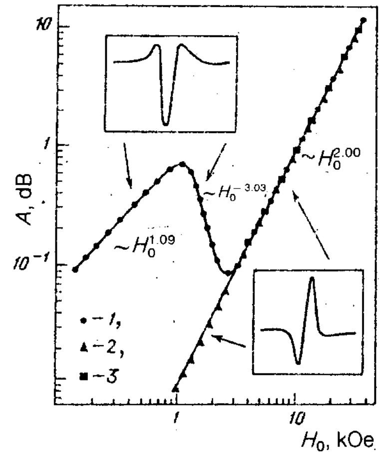

FIG. 6. Magnetic field dependences of the amplitudes of acoustic resonant features in the surface impedance of plane-parallel plates of 3d magnets: *1*—Inconel, *2*—nickel, *3*—coronel. Inserts show the shapes of these acoustic resonances at field values corresponding to magnetoelastic and inductive interactions.[58]

3. GENERATION OF LONGITUDINAL ULTRASOUND IN FERROMAGNETS BY THE MOTION OF DOMAIN WALLS

It is well known that a transition metal in the ferromagnetic state is divided into domains within which the magnetization is nonzero. Between the domains there are regions (domain walls) where the orientation of M varies from one equilibrium orientation to another. If a static magnetic field $\mathbf{H}_0$ is applied the domains that are improperly oriented with respect to this field are absorbed by the domains whose magnetization orientation is close to the direction of the field.

In EAC studies where the static magnetic field is modulated by the ac field, the domain walls within the skin layer experience an oscillatory force. This force causes both bending and rotation-translation of the walls. Each of these processes is accompanied by the excitation of ultrasound. The generation of ultrasound due to uniform displacement of the domain walls in ferrodielectrics was investigated by Turov and Lugovoi.[82] For metals, which are characterized by a very nonuniform distribution of the alternating magnetic field within the skin layer, it seems justified to consider the generation of ultrasound due to bending of domain walls.

In the tangential geometry $\mathbf{H}_0 \| \mathbf{h} \| \mathbf{x}$, $\mathbf{k} \| \mathbf{n} \| \mathbf{z}$ the system of equations describing the excitation of ultrasound due to domain wall bending can be written as

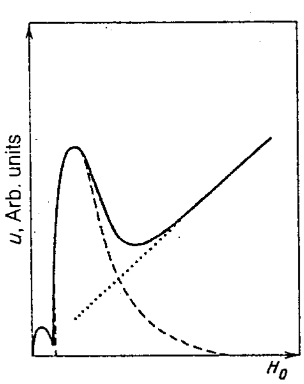

FIG. 5. Magnetic field dependence of the amplitude of surface acoustic wave excitation in polycrystalline iron.[68]

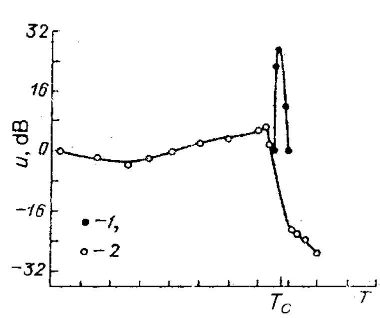

FIG. 7. Temperature dependence of the efficiency of longitudinal (*1*) and transverse (*2*) ultrasound excitation in polycrystalline iron.[81]

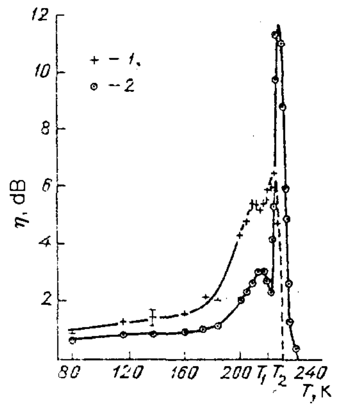

FIG. 8. Temperature dependence of the efficiency of transverse (1) and longitudinal (2) ultrasound excitation in polycrystalline terbium in tangential magnetic field $H_0 = 1.7$ kOe.[61]

$$
\begin{aligned}
& m\ddot{v} + \varkappa v = Mh - \gamma M^2 \frac{\partial U}{\partial z},\\
& \left(k_{\mathrm{A}}^2 + \frac{\partial^2}{\partial z^2}\right) U = -(2\gamma M^2/dS^2)\frac{\partial v}{\partial z},\\
& \left(k_{\mathrm{E}}^2 + \frac{\partial^2}{\partial z^2}\right) h = -8\pi v k_{\mathrm{E}}^2 M/d,
\end{aligned}
\tag{26}
$$

where v is the average displacement of the domain wall, m and $\varkappa$ are the averages of the mass and the elasticity coefficient of the domain wall, and γ and d are the averages of the magnetostriction constant and of the domain dimensions.

Using boundary conditions (12), one can show that the solution of system of equations (26) is given by formulas (22)–(24), where one must substitute the following expressions for the magnetic susceptibility χ and the parameter of the magnetoelastic interaction ξ:

$$
\chi = \frac{\chi_0 \omega_0^2}{\omega_0^2 - \omega^2}, \quad \xi = \frac{\gamma^2 M^2 \chi}{\rho_M S^2}. \tag{27}
$$

Here $\chi_0 = 2M^2/\varkappa d$ is the static susceptibility corresponding to domain wall displacement and $\omega_0 = (\varkappa/m)^{1/2}$ is the eigenfrequency of the domain wall oscillations. In this case, the EAC efficiency depends on the external magnetic field through the quantities d, m, and $\varkappa$, which characterize the domain structure and the domain walls of the sample. According to Eqs. (27), the dynamic susceptibility of the magnet χ, as well as the EAC efficiency, depend resonantly on H_0. Estimates[83] show that ω_0 is in the range of tens and hundreds of megahertz.

4. ELECTROMAGNETIC GENERATION OF ULTRASOUND IN ANISOTROPIC FERROMAGNETS

The mechanisms of electromagnetic-acoustic conversion considered in Sections 2 and 3 cover the problem of excitation of ultrasound in isotropic magnets, polycrystals, and in single crystals with a nonregular domain structure. Further study of the phenomena requires analysis in single-crystal samples with a regular domain structure and in single-domain single crystals. This analysis can be done for any type of crystallographic and magnetic symmetry, but we consider here only the generation of ultrasound in hexagonal ferromagnets in a tangential magnetic field. This choice is motivated by the fact that the most detailed study of EAC has been performed for that type of crystals.[64,66]

The magnetization processes are different for the different orientations of the static magnetic field $\mathbf{H}_0$ with respect to crystallographic axes of a metal. In small fields the magnetization is mainly due to the displacement of domain walls. After this process is over three qualitatively different states of ferromagnet can be established. If the magnetic field $\mathbf{H}_0$ is oriented along the easy axis of ferromagnet, the latter becomes single-domain with the magnetization $\mathbf{M}$ parallel to $\mathbf{H}_0$ and its further magnetization is only due to the paraprocess. In a magnetic field oriented along the hard axis of a ferromagnet there remain two types of domains, and further magnetization occurs via rotation of the magnetic moments within domains. In the intermediate case the ferromagnet becomes a single domain, with the vector $\mathbf{M}$ at some angle to $\mathbf{H}_0$ and its further magnetization comes about by aligning $\mathbf{M}$ with $\mathbf{H}_0$. Since as all the features of the inductive mechanism of conversion remain unchanged in single crystals we consider below only the specifics of magnetoelastic mechanism of EAC.

4.1. Generation of longitudinal ultrasound in magnets by rotation of magnetic moments (spin-flip transitions)

Thus, in some range of static magnetic field the real domain structure of a single-crystal ferromagnet can be approximated by two types of domains with magnetizations having components perpendicular to the magnetic field. We shall examine the problem of generation of longitudinal ultrasound for the following case of the mutual orientation of the static, $\mathbf{H}_0$, and ac, $\mathbf{h}$, magnetic fields and wave vector $\mathbf{k}$ of the ultrasound: $\mathbf{k}\|\mathbf{n}\|\mathbf{x}\|\mathbf{a}$, $\mathbf{H}_0\|\mathbf{h}\|\mathbf{y}\|\mathbf{b}$ (here $\mathbf{n}$ is the normal to the surface of the metal and $\mathbf{a}$ and $\mathbf{b}$ are the easy and hard twofold axes in the basal plane of the hexagonal ferromagnet).

The free energy density of a hexagonal two-domain ferromagnet can be expressed in the form

$$
\begin{aligned}
F = \sum_{n=1}^{2} \Big(& \frac{1}{4}K_1 \cos^2\vartheta_n + \frac{1}{8}K_2 \cos^4\vartheta_n + K_6 \sin^6\vartheta_n \cdot \cos 6\phi_n \\
& - \frac{1}{2} MH \sin\vartheta_n \cdot \sin\phi_n \\
& - \frac{1}{2} hM^{(n)} + \frac{1}{2}\gamma_{ijkl} M_i^{(n)} M_j^{(n)} U_{kl} \Big) + C_{ijkl} U_{ij} U_{kl} \\
& + \frac{1}{8} M^2 [N_1 (\sin\vartheta_1 \cdot \cos\phi_1 \\
& + \sin\vartheta_2 \cos\phi_2)^2 + N_2 (\sin\vartheta_1 \cdot \sin\phi_1 + \sin\vartheta_2 \cdot \cos\phi_2)^2 \\
& + N_3 (\cos\vartheta_1 \\
& + \cos\vartheta_2)^2] + \frac{1}{2}\pi M^2 (\sin\vartheta_1 \cdot \sin\phi_1 - \sin\vartheta_2 \cdot \sin\phi_2)^2 .
\end{aligned}
\tag{28}
$$

Here $n = 1, 2$ are the indices of domains, ϑ_n and ϕ_n are the polar and azimuthal angles of the magnetization in the domains with respect to sixfold $\mathbf{c}$ and twofold $\mathbf{a}$ axes, respectively, K_1 and K_2 are the constants of uniaxial magnetic anisotropy, K_6 is the basal plane anisotropy constant, and N_i are the demagnetizing factors of the samples. The next-to-last term in expression (28) is the demagnetization energy, and the last is the energy associated with the presence of magnetic charges on the domain walls.[83]

Let us consider that the spin flip takes place only in the basal plane, as is usually the case for many rare earth magnets because of the giant uniaxial anisotropy.[84] In the investigation of ultrasound generation in magnets with a domain structure, i.e., with inhomogeneous magnetization in the ground state, the system of equations (1)–(4) must be supplemented by the Saint-Venant strain compatibility condition principle,[85] which leads also to inhomogeneous strains in the ground state. However, if the domain wall width is small compared with the period of the domain structure, the magnetization and strains inside the domains can be regarded as homogeneous. In this case for a magnet in the ground state one can write

$$\vartheta_1 = \vartheta_2 = \theta = \pi/2, \quad \phi_1 = \Phi, \quad \phi_2 = \pi - \Phi,$$

$$U_{xx,yy} = -\frac{(\gamma_{11} - \gamma_{12})M^2 c_{33}}{2[c_{33}(c_{11} + c_{12}) - 2c_{13}^2]} + \frac{(\gamma_{11} - \gamma_{12})M^2}{2(c_{11} - c_{12})}\cos 2\Phi, \tag{29}$$

$$U_{zz} = -c_{13}(U_{xx} + U_{yy})/c_{33}, \quad U_{xy} = -\frac{(\gamma_{11} - \gamma_{12})M^2}{2(c_{11} - c_{12})}\sin 2\Phi,$$

$$U_{xz} = U_{yz} = 0.$$

Here the components of the anisotropic magnetostriction tensor γ_{ijkl} are written in the two-index representation.[85]

The azimuthal angle Φ is determined from the equation

$$6K_6\sin 6\Phi + MH_0\cos\Phi - \frac{1}{2}M^2N_2\sin 2\Phi = 0. \tag{30}$$

A change in the magnetic field leads to a change in the magnet ground state. The phase with the domain structure (29) is stable for $H_0 \leqslant H_{th}$, where the threshold field is

$$H_{th} = N_2M - 36K_6/M. \tag{31}$$

At $H_0 = H_{th}$ an orientational second-order transition takes place from a noncollinear state with a domain structure (29) into a collinear single-domain state with $\phi_1 = \phi_2 = \pi/2$.

For the propagation of waves along the x axis, the system of Equations (1)–(4), linearized in the standard manner about the equilibrium position Eqs. (29) and (30), can be written as

$$\left(1 - \frac{1}{2}i\delta^2\frac{\partial^2}{\partial x^2}\right)h_z - 4\pi M\vartheta_+ = 0,$$

$$\left(1 - \frac{1}{2}i\delta^2\frac{\partial^2}{\partial x^2}\right)h_y + 4\pi M\phi_-\cos\Phi = 0,$$

$$-i\omega\phi_+ = \omega_1\vartheta_+ + gh_z,$$

$$-i\omega\vartheta_+ = -\omega_3\phi_+ - g(\gamma_{11} - \gamma_{12})\frac{\partial u_y}{\partial x}M\cos 2\Phi, \tag{32}$$

$$-i\omega\phi_- = \omega_4\vartheta_- - g\gamma_{44}M\frac{\partial u_z}{\partial x}\cos\Phi,$$

$$-i\omega\vartheta_- = -\omega_2\phi_- + gh_y\cos\Phi + g(\gamma_{11} - \gamma_{12})M\frac{\partial u_z}{\partial x}\sin 2\Phi,$$

$$-\rho_M\omega^2u_x = -(\gamma_{11} - \gamma_{12})M^2\frac{\partial\phi_-}{\partial x}\sin 2\Phi + c_{11}\frac{\partial^2u_x}{\partial x^2},$$

where $\vartheta_\pm = (\vartheta_1 \pm \vartheta_2)/2$, $\phi_\pm = (\phi_1 \pm \phi_2)/2$, and the frequencies ω_i are given by the equations

$$\omega_1 = \frac{g}{M}\Big(K_1 - 6K_6\cos 6\Phi + MH_0\sin\Phi - N_2M^2\sin^2\Phi + N_3M^2\Big),$$

$$\omega_2 = \frac{g}{M}[-36K_6\cos 6\Phi + MH_0\sin\Phi + N_2M^2\cos 2\Phi + 2(\gamma_{11} - \gamma_{12})^2M^4/(c_{11} - c_{12})], \tag{33}$$

$$\omega_3 = \omega_2 + 4\pi gM + gM(N_1\sin^2\Phi - N_2\cos^2\Phi),$$

$$\omega_4 = \omega_1 - gMN_3.$$

The system of equations (32) describes both the in-phase (ϑ_+, ϕ_+) and antiphase (ϑ_-, ϕ_-) oscillations of the magnetization in domains. This system becomes much simpler at frequencies $\omega \ll \omega_i$. The assumption of this inequality is equivalent to the statement that the modulation of the static magnetic field by an ac field does not cause a tilt of the magnetization in domains from the basal plane. In this case the electromagnetic wave excites only antiphase oscillations of magnetization ϕ_- and longitudinal elastic waves u_x. Excluding ϕ_- from Eq. (32), one can get for h_y and u_x formulas similar to Eqs. (15) and (16), where it is necessary, however, formally to set $H_0 = 0$, and to use the following expressions for the γ, χ, and ξ

$$\chi = \frac{gM}{\omega_2}\cos^2\Phi = \chi_0\cos^2\Phi, \quad \xi = \frac{\gamma^2M^2\chi}{\rho_M S_1^2}, \tag{34}$$

$$\gamma = 2(\gamma_{11} - \gamma_{12})\sin\Phi.$$

Here S_1 is the velocity of longitudinal ultrasound propagating along the twofold symmetry axis.

The roots of the dispersion equation (16) are the wavevectors q_1 and q_2, which can be determined with the help of Eq. (34) using Eq. (22). The amplitude of the generated ultrasound and the efficiency of EAC are given, as before by Eqs. (23) and (24), where it is necessary to substitute the expressions for μ, χ, and ξ, as given by Eq. (34). All these values depend on the magnetic field because ω_2 and Φ which enter into (34) also depend on H_0. If the parameter ξ is small compared to μ for all values of temperature and magnetic field, then the EAC efficiency can be written as

$$\eta = \text{const}\cdot\frac{\chi_0^2\sin^2\Phi\cdot\cos^4\Phi}{(1 + 4\pi\chi_0\cos^2\Phi)^2}. \tag{35}$$

The frequency ω_2 given by Eq. (33), which figures in χ_0, decreases with increasing magnetic field and reaches a minimum, equal to the value of the magnetoelastic gap $\omega_{ma} = 2g(\gamma_{11} - \gamma_{12})^2 M^3/(C_{11} - C_{12})$ at the orientational phase transition point $H_0 = H_{th}$ ($\Phi = \pi/2$). The susceptibility χ_0 is then at a maximum. In addition, the numerator in Eq. (35) is zero at $\Phi = \pi/2$ and at $\Phi = 0$ and therefore the conversion efficiency has a maximum at $\Phi = \arcsin(1/\sqrt{3})$. Thus, for this domain structure the efficiency with which longitudinal ultrasound is excited is low in weak fields and in fields $H_0 \gg H_{th}$, but reaches a maximum in intermediate fields.

4.2. Experimental investigation of electromagnetic-acoustic conversion in single-crystal ferromagnets

Extensive studies of EAC have been performed on single crystals of 3d-magnets—Cr, Ni, Co, Fe–Si, Ni_2MnGa, and 4f-magnets—Gd, Dy, Er, Tb. In all these metals ultrasound was generated both by the inductive interaction, and the magnetoelastic interaction within the skin layer. The latter resulted either from volume magnetostriction at magnetic phase transitions of various types, or from anisotropic magnetostriction at spin-flip transitions. Not all of these transitions, however, were accompanied by a sharp increase of ultrasound excitation. Consider, for example, the temperature dependence of the efficiency of longitudinal ultrasound excitation in single-crystal Ni_2MnGa, (Ref. 86) shown in Fig. 9. This compound undergoes a ferromagnetic transition at $T_C = 376$ K, and at $T_M = 202$ K it experiences structural transformation of the martensitic type into ferromagnetic state. It is evident that in the region of the structural transition the EAC efficiency η sharply increases, and the hysteretic behavior at this region is characteristic of martensitic transformations. In the temperature range $T_M < T < T_C$ the generation of ultrasound was due to spin-flip processes. The absence of generation of appreciable efficiency at Curie point indicates the small value of the volume magnetostriction of Ni_2MnGa in the vicinity of this point.

The most extensive measurements of the EAC have been conducted on single-crystal samples of nickel,[48,55,87] gadolinium,[63,64] and dysprosium.[65–67] These measurements were conducted not only to study the phenomena of electromagnetic and acoustic wave conversion, but also to obtain information on magnetic parameters of these metals.

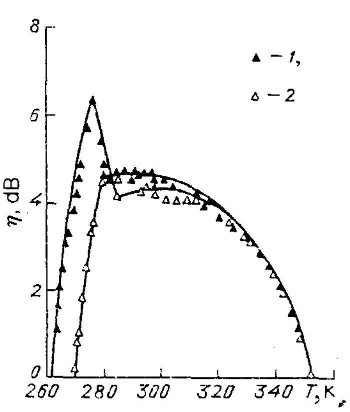

FIG. 9. Temperature dependence of the efficiency of EAC magnetoelastic mechanism in Ni_2MnGa in a field $H_0 = 100$ Oe. ▲ and Δ—increasing and decreasing temperature, respectively.

4.2.1. Nickel

Nickel has a face-centered cubic lattice. It transforms into the ferromagnetic state with the magnetization aligned with the [100] crystal axes at $T_C = 650$ K. At $T_{SF} = 460$ K a spontaneous spin-flip transition takes place, resulting in the rotation of magnetization to the [111] direction. The magnetic anisotropy constants of Ni are relatively small, so that spin flip can be induced by a relatively moderate external magnetic field.

The first experimental studies of EAC in single-crystal nickel showed[48,87] that intense excitation of ultrasound is observed not only in the region of the paramagnetic–ferromagnetic transition, but also in the ferromagnetic state as a result of spin flip. For instance, on the curve of the excitation efficiency of longitudinal ultrasound, shown in Fig. 10, we see a pronounced peak in the temperature region where the spins undergo a spontaneous flip from the [111] to the [100] direction.

The EAC field dependences, as shown in Figs. 11 and 12, are very nonmonotonic. The peak in the curves of $\eta(H_0)$ are due to the field-induced spin flip, while in the stronger field the inductive mechanism of transformation appears. The resonance features on the curve of $\eta(H_0)$ shown in Fig. 12 are very prominent, since the corresponding measurements[55] were carried out with a spherical sample, in which the internal field is homogeneous. The study of the field dependences of the efficiency of longitudinal ultrasound generation at various temperatures permits us to determine the temperature dependence of Ni magnetic anisotropy constant K_1, (Ref. 55) which is shown in Fig. 13.

4.2.2. Gadolinium

Gadolinium has a hexagonal lattice and goes from the paramagnetic to the ferromagnetic state of the easy axis type at $T_C = 293$ K. The magnetization vector M coincides in direction with the hexagonal crystal **c** axis in the range $T_{SF} < T < T_C$. At $T_{SF} = 235$ K a cone of easy magnetization axes is formed. As the temperature is lowered, the opening angle of the cone relative to the hexagonal axis first increases rapidly, reaches a maximum at $T \approx 180$ K, and then decreases monotonically. The magnetic anisotropy in gadolinium is small compared to other heavy rare-earth metals, so that spin-flip transitions can be achieved in relatively small magnetic fields. This magnetic structure, which is different, in fact, from the "two-domain" ferromagnet considered above, nevertheless can be described by the formalism given in Sec. 4.1.

The $\eta(T)$ curves for various values of the field $\mathbf{H}_0 \| \mathbf{h} \| \mathbf{a}$

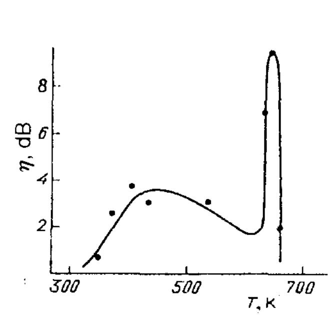

FIG. 10. Temperature dependence of the efficiency of excitation of longitudinal ultrasound in single-crystal Ni.[48]

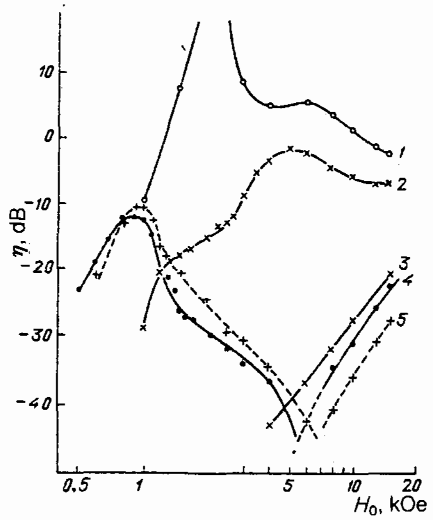

FIG. 11. Magnetic field dependences of the efficiencies of excitation of transverse (*1–3,5*) and longitudinal (*4*) ultrasound in single-crystal Ni at $\omega/2\pi = 6.2$ MHz, $T = 293$ K.[87] *1*—$\mathbf{H}_0 \| [110]$, $\mathbf{h} \| [1\bar{1}0]$; *2*—$\mathbf{H}_0 \| [110]$, $\mathbf{h} \| [001]$; *3*—$\mathbf{H}_0 \| [110]$, $\mathbf{h} \| [1\bar{1}0]$, but $T = 365$ °C (above the Curie temperature); *4*—$\mathbf{H}_0 \| [001]$, $\mathbf{h} \| [001]$; *5*—$\mathbf{H}_0 \| [001]$, $\mathbf{h} \| [110]$.

are shown in Fig. 14. The efficiency of excitation of longitudinal ultrasound in all cases reaches a clearly marked maximum in the region of the transition from the paramagnetic to the ferromagnetic state and falls off away from T_C. In addition, comparable generation efficiency is observed in a certain magnetic field range at low temperatures (curve *2* of Fig. 14). Of interest is the amplitude of the EAC peak as a function of the static magnetic field near the Curie point. This dependence is shown in Fig. 15. One can see that the generation efficiency at the Curie point first increases with the magnetic field, reaches its maximum value, and then decreases. This behavior, in accordance with Eq. (24), is due to the evolution with the magnetic field of $\chi(T)$ and $M(T)$. In weak magnetic fields the susceptibility χ reaches its highest value at the Curie point, but the magnetization is small. In a strong magnetic field, conversely, the magnetization is large, but the susceptibility decreases.

The field dependences of the electromagnetic-acoustic conversion efficiency in the rare-earth metals are of a remarkable variety. Some of these curves for two orientations of the field $\mathbf{H}_0$ relative to the crystallographic axes of Gd: $\mathbf{H}_0 \| \mathbf{h} \| \mathbf{a}$ and $\mathbf{H}_0 \| \mathbf{h} \| \mathbf{c}$, are shown in Figs. 16 and 17.

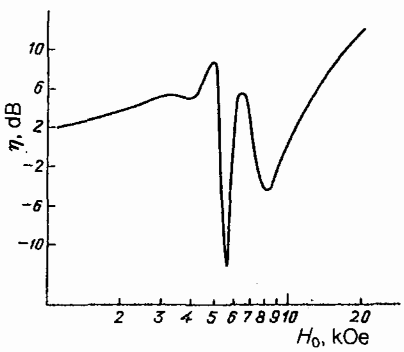

FIG. 12. Magnetic field dependence of the efficiency of longitudinal ultrasound excitation in single crystal Ni at $\omega/2\pi = 15$ MHz, $T = 293$ K; $\mathbf{q} \| [001]$, $\mathbf{H}_0 \| \mathbf{h} \| [110]$.[55]

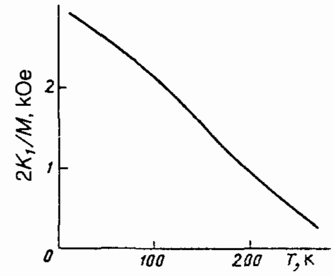

FIG. 13. Temperature dependence of the magnetic anisotropy effective field $2K_1/M$.[55]

For the geometry $\mathbf{H}_0 \| \mathbf{h} \| \mathbf{a}$ near the transition from the paramagnetic to the ferromagnetic state, the generation of ultrasound starts from zero magnetic field, reaches a maximum for $H_0 \sim 2$ kOe and then decreases monotonically (curve *1* of Fig. 16). In the temperature interval $T_{SF} < T < T_C$ generation also starts in weak magnetic fields, reaches a maximum and then falls rapidly and reaches a level weakly dependent on the magnetic field for $H_0 \geqslant 10$ kOe (curve *2* of Fig. 16). Finally, for $T < T_{SF}$ the excitation of ultrasound is observed only in a narrow range of magnetic field H_1–H_2 (curve *3* of Fig. 16). With a change in temperature, both the width of the range and the values of limiting fields H_1 and H_2 change appreciably.

The only difference of the field dependences for the geometry $\mathbf{H}_0 \| \mathbf{h} \| \mathbf{c}$ from the case discussed above is that ultrasound generation in the range $T_{SF} < T < T_C$ starts in a field $H_1 \neq 0$ (curve *2* of Fig. 17).

The dependence of the amplitude of generation of longitudinal ultrasound in Gd over a wide magnetic field range is shown in Fig. 18. In weak fields there is a region of intense generation due to the magnetoelastic interaction. The increase in the amplitude of the detected signal in strong fields is due to the inductive interaction. It can be seen that the efficiency of the inductive conversion mechanism becomes comparable with the efficiency of the magnetoelastic mechanisms in sufficiently strong magnetic fields.

Overall, the results of the investigation of electromagnetic-acoustic conversion in gadolinium can be interpreted in the following way: that over a wide range of variation of magnetic field and temperature the generation of ultrasound

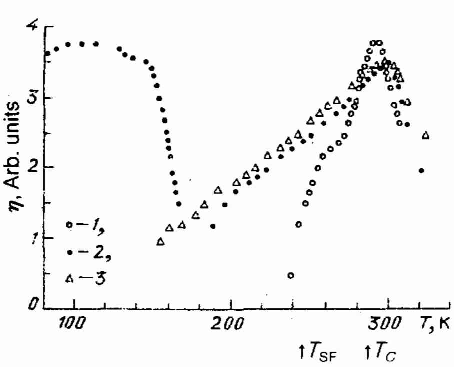

FIG. 14. Temperature dependence of the efficiency of excitation of longitudinal ultrasound in Gd at fixed values of an external magnetic field $\mathbf{H}_0 \| \mathbf{h} \| \mathbf{a}$: *1*—2.2 kOe, *2*—4.4 kOe, *3*—6.7 kOe.[64]

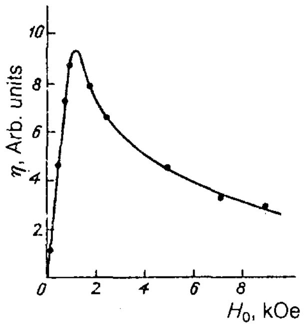

FIG. 15. Magnetic field dependence of the amplitude of longitudinal ultrasound generation peak at paramagnetic–ferromagnetic transition in Gd: $\mathbf{H}_0 \| \mathbf{h} \| \mathbf{a}$.[63]

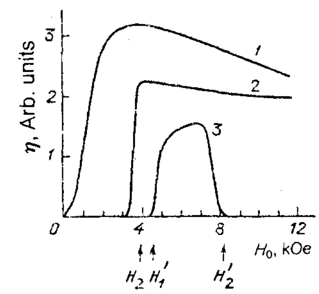

FIG. 17. Magnetic field dependences of the EAC efficiency in Gd: $\mathbf{H}_0 \| \mathbf{h} \| \mathbf{c}$. *1*—$T = 293$ K, *2*—260 K, *3*—80 K.[64]

occurs as a result of the Lorentz force and by the isotropic magnetostriction of the paraprocess and anisotropic magnetostriction associated with spin-flip transitions. To a first order approximation these magnetoelastic interactions can be considered independent of one another, while their contributions to the processes of EAC are additive. Assuming that the conversion due to the paraprocess in single crystals is the same as in polycrystalline material, let us go to the analysis of the conversion efficiency due to spin flip. In order to explain the experimentally observed dependences in the ferromagnetic region it is essential to take account of the real domain structure and of the demagnetization factor of the specimens, as well as the orientation of the field with respect to crystallographic axes. The paraprocess is insignificant far from the Curie temperature and generation takes place only in some interval of magnetic fields limited from above and below, $H_1 < H_0 < H_2$. The absence of generation of ultrasound in fields $H_0 < H_1$ can be explained by the fact that so long as the specimen contains domains unfavorably distributed relative to H_0, the internal magnetic field in the magnetic material is zero. In fields $H_0 < H_1$ an increase in the strength of the static magnetic field and its modulation by the field of the electromagnetic wave only leads to a shift of the domain walls and to a change in the ratio of domains with different directions of the spontaneous magnetization vector. The magnetic susceptibility associated with a shift of domain walls in Gd is apparently small, which leads to a low conversion efficiency. In the range of magnetic fields $H_1 < H_0 < H_2$ the magnetization vector $\mathbf{M}$ rotates away from the direction of spontaneous magnetization to the direction of the external field $\mathbf{H}_0$. This process, in accord with formulas (24) and (35), is accompanied by a sharp increase in the conversion efficiency. Finally, in fields $H_0 > H_2$ ultrasound is no longer generated by spin flip and occurs only via the paraprocess, with an intensity that decreases as the temperature is reduced.

The case $T_{SF} < T < T_C$ for gadolinium is of interest. If $\mathbf{H}_0$ is directed along the easy magnetization axis, the *c* axis, then in the field H_1 the specimen goes over into the single-domain phase in which $\mathbf{M} \| \mathbf{H}_0$, i.e., H_1 coincides with H_2. In this case, although generation also starts at H_1, it takes place only through magnetostriction in the paraprocess (curve *2* of Fig. 17). If the field $\mathbf{H}_0$ lies in the basal plane of the crystal, spin flip starts from zero magnetic field (curve *2* of Fig. 16).

The values of critical fields H_1 and H_2 for which the efficiency of the conversion shows sharp changes, undergo substantial changes with changing temperature. These values for the orientations of the static magnetic field along the hexagonal axis ($\mathbf{H}_0 \| \mathbf{c}$), and in the basal plane ($\mathbf{H}_0 \| \mathbf{a}$) are shown in Figs. 19 and 20, respectively. It can be shown that from $H_1(T)$ and $H_2(T)$ one can reconstruct the magnetic phase diagrams of gadolinium; that is, determine the regions of existence of the polydomain, canted (the magnetization $\mathbf{M}$ not parallel to the field $\mathbf{H}_0$), and collinear ($\mathbf{M} \| \mathbf{H}_0$) phases.

Let us write that part of the free energy density of the crystal which depends on the angle ϑ between the direction of magnetization $\mathbf{M}$ and the $\mathbf{c}$ axis:

$$F = (1/2)K_1 \cos^2\vartheta + (1/2)K_2 M^2 \cos^4\vartheta + (1/2)K_3 M^4 \cos^6\vartheta - \mathbf{H}_i \mathbf{M}, \tag{36}$$

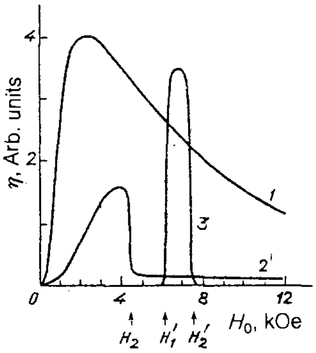

FIG. 16. Magnetic field dependences of the EAC efficiency in Gd: $\mathbf{H}_0 \| \mathbf{h} \| \mathbf{a}$. *1*—$T = 293$ K, *2*—$T = 260$ K, *3*—127 K.[64]

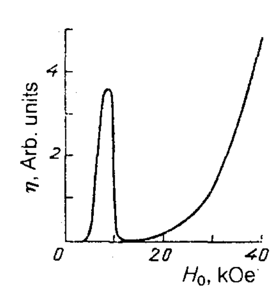

FIG. 18. Magnetic field dependence of the EAC efficiency in Gd: $\mathbf{H}_0 \| \mathbf{h} \| \mathbf{c}$, $T = 80$ K.[64]

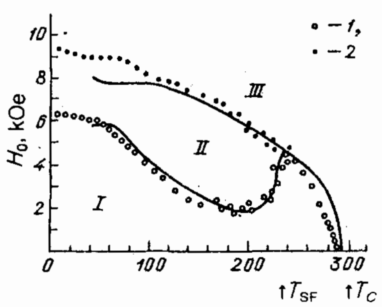

FIG. 19. H_0–T phase diagram of Gd for $\mathbf{H}_0 \| \mathbf{c}$. *1*—$H_1$, *2*—$H_2$—experimental points, curves—theory. Regions *I*, *II*, and *III* correspond to single-domain angular, and collinear ferromagnetic phases.[64]

where H_i is the internal magnetic field.

We shall first consider the case of the magnetic field parallel to the hexagonal axis $\mathbf{H}_0 \| \mathbf{h} \| \mathbf{c}$. The processes of domain wall displacement in the specimen end at

$$H_1 = NM \cos \vartheta, \tag{37}$$

where N is the demagnetization factor. In the temperature interval $T_{SF} < T < T_C$ the angle ϑ is equal to zero and the specimen immediately goes over from the polydomain into the collinear phase (i.e., $H_1 = H_2$). For $T < T_{SF}$ the angle ϑ of the cone of easy axes is non-zero and is temperature dependent. A reorientation of the magnetic moments of the atoms to the direction of $\mathbf{H}_0$ starts from the field H_1 and gadolinium is then in the canted phase. The reorientation ends at the field H_2 and gadolinium goes over into the collinear phase. By minimizing F of Eq. (36) with respect to ϑ and assuming then that $\vartheta = 0$, one can find an expression for the second critical field H_2:

$$H_2 = NM + (K_1 + 2K_2M^2 + 3K_3M^4)M^{-1}. \tag{38}$$

In the situation where the static magnetic field lies in the basal plane $\mathbf{H}_0 \| \mathbf{h} \| \mathbf{a}$, the processes of domain wall displacement end at the field

$$H_1 = NM \sin \vartheta. \tag{39}$$

In the interval $T_{SF} < T < T_C$ we have $\vartheta = 0$ and $H_1 = 0$. Unlike the case considered above ($\mathbf{H}_0 \| \mathbf{c}$), in this geometry spin flip occurs over the whole temperature range. Rotation of the magnetic moments ends in the field

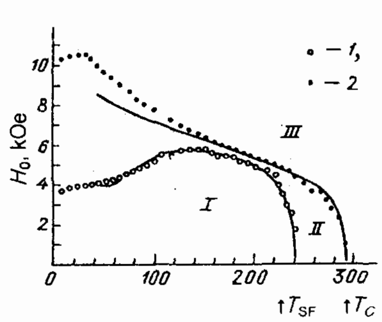

FIG. 20. H_0–T phase diagram of Gd for $\mathbf{H}_0 \| \mathbf{a}$. *1*—$H_1$, *2*—$H_2$—experimental points, curves—theory. Regions *I*, *II*, and *III* correspond to polydomain, canted, and collinear ferromagnetic phases.[64]

$$H_2 = NM - (K_1/M). \tag{40}$$

Calculations of the temperature dependences of the critical fields H_1 and H_2 shown in Figs. 19 and 20 by the solid lines were carried out with the use of data for K_i and M published in Ref. 84. Let us discuss the calculation of the demagnetizing factors N of the samples in electromagnetic/acoustic conversion. Since the ultrasound is generated in a thin near-surface layer the demagnetizing factors must be calculated for fields that act on the surface of the crystal. It can be seen that there is good agreement between experiment and theory in the entire temperature range studied.

4.2.3. Dysprosium

Dysprosium has a hexagonal crystal structure. The uniaxial anisotropy of Dy is so strong that when it is magnetically ordered the moments are always oriented in the basal plane. As the temperature increases in the absence of a static magnetic field, dysprosium goes from a ferromagnetic phase of the easy-plane type at $T_1 = 85$ K into a helicoidal antiferromagnetic phase of the simple helix type, and then at $T_2 = 180$ K into the paramagnetic phase. For $T < T_1$, application of a magnetic field in the basal plane leads to the usual ferromagnet magnetization process produced by displacement of the domain walls and rotation of the magnetization vectors within domains. In the interval $T_1 < T < T_2$ application of a sufficiently strong magnetic field destroys the antiferromagnetic helicoid. Investigations of the influence of a magnetic field oriented along the *a* axis on the magnetization,[88] conductivity,[89] and the velocity of ultrasound[90] in Dy have shown that destruction of the antiferromagnetic helix is accompanied by the formation of an intermediate ferromagnetic fan phase.

Let us consider the results of the study of the processes of longitudinal ultrasound generation in single-crystal dysprosium. Families of characteristic field dependences of the conversion efficiency, obtained for two orientations of the static and ac magnetic fields along easy ($\mathbf{H}_0 \| \mathbf{h} \| \mathbf{a}$) and hard ($\mathbf{H}_0 \| \mathbf{h} \| \mathbf{b}$) axes in the basal plane, are shown for a number of temperatures in Figs. 21 and 22, respectively. Figure 21 shows also the typical field dependences $M(H_0)$. The $\eta(H_0)$ curves are drawn to various scales, and the attenuation coefficients in dB are indicated in the figure captions for each curve.

We consider first the $\eta(H_0)$ curves obtained in the ferromagnetic phase of dysprosium for $T < T_1$ (curve *1* in Fig. 21 and curves *1* and *2* in Fig. 22). For $\mathbf{H}_0 \| \mathbf{h} \| \mathbf{a}$ only one generation peak is observed in the region of relatively weak magnetic fields. The EAC signal appears in the field H_1 practically simultaneously with the application of the magnetic field ($H_1 = 0$), reaches a maximum at $H_0 \sim 10$ kOe, and then decreases rapidly. In a magnetic field oriented along the hard magnetization axis $\mathbf{H}_0 \| \mathbf{h} \| \mathbf{b}$, the field dependence of the conversion shows, following the generation peak in weak fields ($H_0 \sim 10$ kOe), intense generation in a wide range of magnetic fields, which terminates in the field H_2. The value of this field increases rapidly as the temperature is lowered. The field dependence of the magnetization for $T < T_1$ is practically the same for the two orientations of H_0 relative to the crystallographic axes of dysprosium. In a weak field the magnetization undergoes rapid growth that

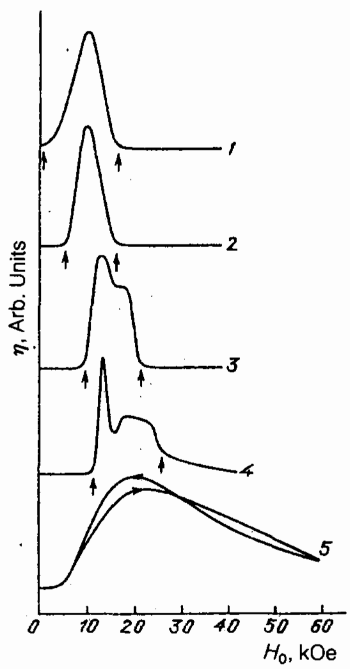

FIG. 21. Magnetic field dependence of EAC efficiency in Dy for $\mathbf{H}_0 \| \mathbf{a}$. *1*—$T = 82$ K, *2*—119 K, *3*—141 K, *4*—172 K, *5*—181 K. Arrows denote magnetic fields H_1 and H_2, which corresponds to beginning and termination of efficient generation of ultrasound.[66]

ends in a field approximately corresponding to the EAC maximum in weak fields, after which the $M(H_0)$ curve reaches saturation (curve *3* of Fig. 22).

The interpretation of the EAC field dependences for $T < T_1$ can be reduced qualitatively to the following. In the customarily assumed weak field the sample contains six types of domain, and the internal field in the magnet is weak.

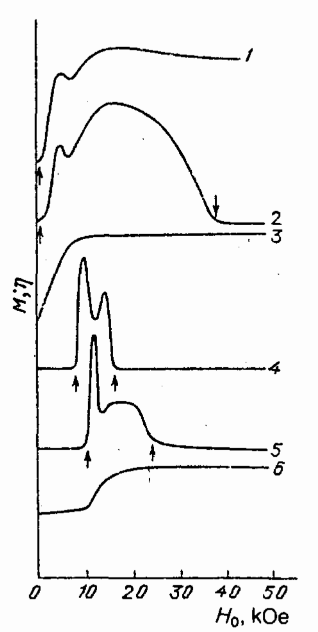

FIG. 22. Magnetic field dependence of EAC efficiency η and magnetization M in Dy for $\mathbf{H}_0 \| \mathbf{b}$. $\eta(H_0)$: *1*—$T = 50$ K, *2*—70 K, *4*—136 K, *5*—173 K. $M(H_0)$: *3*—$T = 70$K, *6*—173 K. Arrows denote magnetic fields H_1 and H_2.[66]

Generation of longitudinal ultrasound for $\mathbf{H}_0 \| \mathbf{h} \| \mathbf{a}$ is due only to domain-wall displacements. When the magnetic field is increased, the volume of domain for which $\mathbf{M} \| \mathbf{H}_0$ increases, and the volume of the domains in which the vector $\mathbf{M}$ is either antiparallel to $\mathbf{H}_0$, or makes an angle with it decreases. Modulation of the static magnetic field by an rf field in the skin layer of the sample leads, on account of the magnetoelastic coupling, to excitation of ultrasound. After the sample goes over into the collinear single-domain phase, the sample is magnetized to saturation and the conversion efficiency decreases steeply.

In the $\mathbf{H}_0 \| \mathbf{h} \| \mathbf{b}$ orientation the sample magnetization should in principle, be completed by aligning the magnetization vector $\mathbf{M}$ in the domain with the direction of the hard axis $\mathbf{b}$. The sequence of the ensuing changes of the magnetic state of dysprosium is the following. The displacement processes, as in the preceding case, lead to excitation of ultrasound and to the appearance of a peak on the $\eta(H_0)$ curve in the region of weak magnetic fields. After the displacement processes terminate, there remain in the sample two types of domain, in which the vector $\mathbf{M}$ makes an angle 30° with the magnetic field. Additional magnetization of the crystal, up to the field H_2, is due to rotation of the vectors $\mathbf{M}$ within these domains. Thus, the second maximum on the field dependences of the EAC efficiency in the $\mathbf{H}_0 \| \mathbf{h} \| \mathbf{b}$ orientation (curves *1* and *2* of Fig. 22) is due to the spin flip in the canted phase. In accordance with the analysis given above, this process should terminate at the field H_{th} given by Eq. (31). Since the easy-plane magnetic anisotropy of Dy rapidly increases as the temperature is reduced, the spin-flip transition point can be reached only in a restricted temperature range (cf. curves *1* and *2* of Fig. 22). Physically, the threshold field H_{th} corresponds to the experimentally determined field H_2. The temperature dependence of this field, as follows from Eq. (31), allows us to determine the temperature dependence of the easy-plane anisotropy constant $K_6(T)$.

In the temperature interval $T_1 < T < T_2$ the general features of the $\eta(H_0)$ curves (curves *2–4* of Fig. 21 and curves *4, 5* of Fig. 22) change considerably. In this interval the shape of $M(H_0)$ (curve *6* of Fig. 22) changes as well. In weak fields, up to a certain temperature-dependent value H_1, the magnetization changes little, and no excitation of ultrasound is observed. This is in accord with Eq. (24), which shows that the excitation efficiency is low in this region. When the field H_1 is reached, the slope of the $M(H_0)$ curve increases abruptly and an EAC signal appears discontinuously. After the $\eta(H_0)$ peak, there can be observed near H_1 an entire region of intense excitation of ultrasound, extending all the way to the field H_2, which is also temperature-dependent. No conversion is detected in fields stronger than H_2, and the magnetization saturates. The field dependences of the electromagnetic-acoustic conversion of this type are typical of both investigated orientations of the external magnetic field.

The $\eta(H_0)$ and $M(H_0)$ curves obtained for $T_1 < T < T_2$ offer evidence that the destruction of the antiferromagnetic helicoid goes through two stages. The sequence of the magnetic states is then the following: for $H_0 < H_1(T)$ the antiferromagnetic helix persists, while in fields $H_0 \geqslant H_1(T)$ it is destroyed and an intermediate ferromagnetic phase is formed and persists up to the field $H_2(T)$.

In fields $H_0 > H_2(T)$ all the magnetic moments take the direction of the magnetic field and the sample is magnetized to saturation. One should accordingly observe on the field dependence of the magnetization slight slope changes, while the $\eta(H_0)$ curves should show peaks of ultrasound generation when the antiferromagnetic helix and the region of intense ultrasound generation due to spin flip in the intermediate ferromagnetic phase are destroyed.

A natural question concerns the nature of the intermediate ferromagnetic phase. In a field $\mathbf{H}_0 \| \mathbf{h} \| \mathbf{b}$ for $T < T_1$, the canted phase is certainly produced after the completion of the displacement, and a fan phase is realized at $T \leqslant T_2$—after the destruction of the antiferromagnetic helicoid. There should exist, therefore, between these two phases a separation region (or boundary). To find this boundary, detailed measurements of the electromagnetic-acoustic conversion were undertaken near T_1 (Ref. 68). Their distinctive feature, as shown in Fig. 23, is the appreciable hysteresis which is absent at other temperatures. It can be proposed that the line on the H_0–T diagram that separates the regions with and without hysteresis on the $\eta(H_0)$ plot is the boundary of the canted phase.

Finally, for $T > T_2$, the conversion plots show one broad generation maximum whose value decreases with increasing distance from T_2 (curve 5 of Fig. 21). This behavior is typical of the paramagnetic phase of any magnet, and its interpretation is the same as for gadolinium. Note that near T_2 the paramagnetic phase of Dy also has hysteresis on the EAC field dependences.

In principle, the magnetic phase diagram of dysprosium can be determined from experimental data on electromagnetic generation of ultrasound in the same way as for gadolinium. The experimental values of the critical fields H_1 and H_2 in the temperature range which includes both the antiferromagnetic and ferromagnetic ordering in this metal for the $\mathbf{H}_0 \| \mathbf{h} \| \mathbf{a}$ and $\mathbf{H}_0 \| \mathbf{h} \| \mathbf{b}$ orientations are shown in Figs. 24 and 25. Unlike gadolinium, however, dysprosium has a relatively large easy-plane magnetic anisotropy, so that it is necessary in addition to calculate the helicoidal antiferromagnetic structure to plot the theoretical curves of the critical magnetic field.

A calculation of such a structure in a hexagonal crystal without allowance for anisotropy in the easy plane was carried out earlier in Ref. 91. The magnetic moments of each crystal plane, coupled by the strong exchange interaction, were described by a single azimuthal angle ϕ_i. A ferromagnetic exchange interaction was assumed between neighboring planes, and an antiferromagnetic interaction was assumed between every other plane. It follows from this model that the destruction of the helicoidal structure by a magnetic field proceeds in two stages: in a field H_1 the helicoid is abruptly destroyed and a ferromagnetic fan structure is produced; with further increase of the field the fan angle decreases, and in a field $H_2 = 2.06H_1$ the magnetic moments of the atoms are oriented along $\mathbf{H}_0$. From the experimental data[66,67] it follows, however, that for $\mathbf{H}_0 \| \mathbf{a}$ the destruction of the helicoid is not always accompanied by formation of a fan structure—at temperatures below 125 K the fan phase is apparently not realized in this orientation. At the same time, for $T > 125$ K the calculation[91] is in satisfactory agreement with experiment.

It can be proposed that the vanishing of the fan phase as T_1 is approached is connected with the influence of the easy-plane anisotropy, which increases rapidly when the temperature is lowered.[92] Since the period of the helicoid in Dy is about ten lattice periods, an analytic calculation of such a structure with allowance for easy-plane anisotropy is quite complicated. Numerical methods were therefore used to find the energetically most favorable spin configuration.

The expression for the free energy f in dimensionless variables can be written as follows

$$f = \sum_i \{-\cos(\phi_i - \phi_{i-1}) + j\cos(\phi_i - \phi_{i-2}) - l\cos\phi_i + k_6\cos[6(\phi_i - \psi)]\}, \qquad (41)$$

where ϕ_i is the angle between the direction of the magnetic moments in ith layer and an external magnetic field,

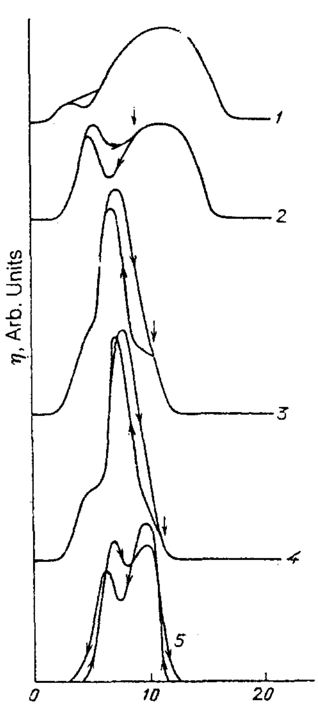

FIG. 23. Magnetic field dependence of EAC efficiency in Dy for $\mathbf{H}_0 \| \mathbf{b}$ near the boundary of coexistence of the canted and fan phases. 1—$T = 91$ K, 2—92 K, 3—98.5 K, 4—101 K, 5—119 K. Arrows denote fields where the hysteretic processes terminate.[66]

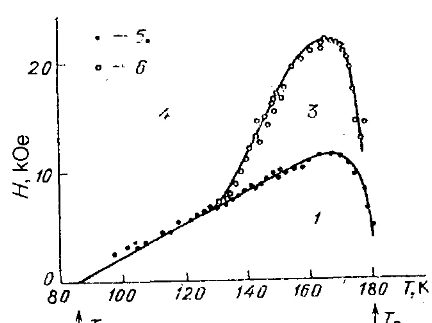

FIG. 24. H_0–T phase diagram of Dy for $\mathbf{H}_0 \| \mathbf{a}$. 1—helicoid, 3—fan, 4—collinear phase. 5—H_1, 6—H_2—experimental points, curves—theory.[66]

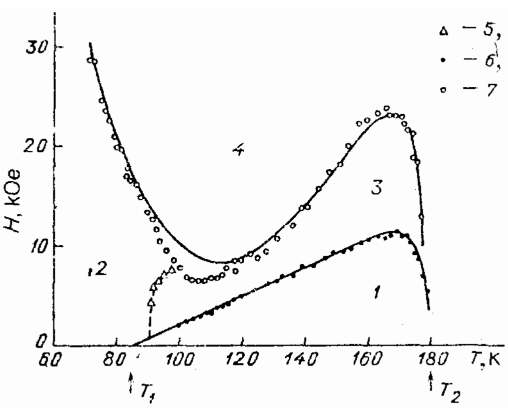

FIG. 25. H_0–T phase diagram of Dy for $\mathbf{H}_0 \| \mathbf{b}$. 2—canted phase. 5–7—experimental points, curves—theory.[66]

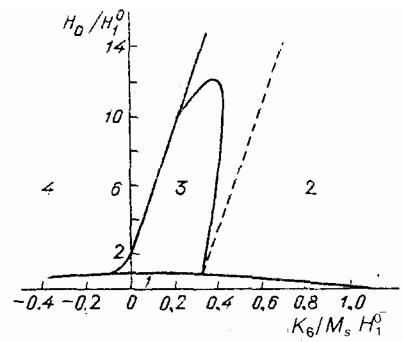

FIG. 26. Phase diagram of Dy for $\psi = 30°$ ($\mathbf{H}_0 \| \mathbf{a}$) for $K_6 < 0$, and for $\psi = 2/3°$ with $K_6 > 0$. 1—helicoid, 2—canted, 3—fanfold, 4—collinear phase. Dashed line is the boundary between fan and canted phases at $\psi = 0°$ ($\mathbf{H}_0 \| \mathbf{b}$).[66]

$j = I_2/I_1$, I_1 and I_2 are the Enz's exchange integrals,[91] $l = H_0/I_1 M$ and $k_6 = K_6/I_1 M^2$ are the renormalized magnetic field and easy-plane anisotropy constant, respectively, and ψ is the angle between the direction of $\mathbf{l}$ and the $\mathbf{b}$ axis of the basal plane. The value $j = (1/4)\cos(2\pi/11)$ was specified so that in the absence of anisotropy and of a magnetic field a helicoid with a period equal to 11 lattice periods arose. This corresponds to Dy at $T = 105$ K, where the easy-plane anisotropy constant K_6 is already quite large ($\sim 10^5$ erg·cm^{-3} (Ref. 92).

With the use of Eq. (41) the phase diagrams of dysprosium were calculated for the following orientations of the external magnetic field H_0 in the basal plane: $\psi = 0°$, $2/3°$, $30°$ (the last—for $\mathbf{H}_0 \| \mathbf{a}$, the transition from $\psi = 0°$ to $30°$ is equivalent to the reversal of the sign of k_6).

Figure 26 shows these diagrams for $\psi = 2/3°$ (i.e., a small deviation from the hard axis $\mathbf{b}$) for $K_6 > 0$, and for $\psi = 30°$ for $K_6 < 0$. It can be seen that with an increase of the anisotropy the helicoidal structure is suppressed and for $K_6/H_1^0 M \approx 1$ it is not realized at all (H_1^0 is the value of H_1 at $K_6 = 0$, i.e., the value used in the initial model[91]). A collinear ferromagnetic structure occurs at

$$H_2 = 2{,}06 H_1^0 + (36 K_6/M). \tag{42}$$

It has turned out that the boundary between the fanfold and canted phases is extremely sensitive to the misorientation ψ of the magnetic field relative to the hard axis. The dashed line in Fig. 26 shows this boundary for $\psi = 0°$; all the remaining phase boundaries at $\psi = 0°$ and $2/3°$ are practically the same.

It is seen from Fig. 26 that for $\mathbf{H}_0 \| \mathbf{b}$ the helicoidal-canted-fan triple point is determined by the condition $K_6/H_1^0 M \approx 0.3$. Control calculations for the values of j corresponding to helicoid periods equal to 18 and 9 lattice periods have shown that the general structure of the H_0–K_6 phase diagrams is preserved, and the values of $K_6/H_1^0 M$, corresponding to the triple point and to total suppression of the helicoidal structure, differ by less than 10%. Thus, one can expect the foregoing conclusion to be valid for any real value of the helicoid period.

The foregoing interpretation of the field dependences of the conversion efficiency can be used to construct the magnetic phase diagrams of Dy in a magnetic field oriented along the easy and hard axes in the basal plane. To establish the boundaries of existence of various magnetic states, the internal magnetic field H_i in the sample was calculated with allowance for the temperature dependences of both the saturation magnetization and the easy-plane anisotropy constants.[84]

The magnetic phase diagrams of dysprosium constructed in this manner for $\mathbf{H}_0 \| \mathbf{a}$ and $\mathbf{H}_0 \| \mathbf{b}$ are shown in Figs. 24 and 25, respectively. With the internal magnetic field and temperature as coordinates, the boundary of the polydomain phase below T_1 practically coincides with the horizontal axis ($H_i \ll 1$ kOe). The lower curve in Fig. 24 for $T_1 < T < T_2$ is the limit of existence of the antiferromagnetic phase, while the upper curve is the limit of existence of the ferromagnetic fan phase. The upper curve in Fig. 25 shows the $H_2(T)$ dependence calculated from Eq. (42). The phase diagram for $\mathbf{H}_0 \| \mathbf{b}$ also shows the boundary between the fan and the canted ferromagnetic phase. This boundary was constructed with the field dependences shown in Fig. 23, and corresponds to the fields and temperatures of the completion of the hysteresis processes in the curve of $\eta(H_0)$. The canted phase is to the left of this boundary and the fan phase is to the right. We note that according to the above estimate, the triple point on the phase diagram of the antiferromagnetic helicoid/ferromagnetic fan/ferromagnetic canted phases should occur at $T \approx 90$ K. The experimentally observed boundary is in fact near this temperature.

The experimental and theoretical curves for the critical magnetic fields are in good agreement, and hence we can regard the technique of electromagnetic-acoustic conversion as a new method of determining the boundaries of various magnetic states in ferromagnets.

5. RESONANT GENERATION OF TRANSVERSE ULTRASOUND IN SINGLE-DOMAIN FERROMAGNETS

In general, the system of equations of interacting electromagnetic, spin, and elastic waves, Eqs. (1)–(4), describes generation of both longitudinal and transverse ultrasound. In the preceding sections we considered mainly the excitation of longitudinal elastic waves, although the processes of domain walls displacement or spin flip can be accompanied by the excitation of transverse ultrasound with comparable efficiency. The only exception to the rule is the magnetoelastic generation due to isotropic magnetostriction, which does not result in transverse ultrasound excitation.

The generation efficiency of various types of elastic waves depends on the orientation of the static magnetic field with respect to the surface of a metal. In a tangential magnetic field both longitudinal and transverse ultrasonic waves are excited, while the possible situations in a magnetic field $\mathbf{H}_0$ perpendicular to the surface permit excitation only of transverse ultrasound.

Let us consider the generation of transverse ultrasound in a hexagonal crystal situated in a normal magnetic field and magnetized along the sixfold $\mathbf{c}$ axis. Let the vector of the static magnetic field $\mathbf{H}_0$ coincide with this axis ($\mathbf{H}_0 \| \mathbf{c}$), while the vector of the ac magnetic field $\mathbf{h}$ lies in the basal plane and is oriented along the twofold axis $\mathbf{a}$ ($\mathbf{h} \| \mathbf{a}$). In this case the static magnetic field is modulated in angle but not in magnitude. The magnetic state with $\mathbf{M} \| \mathbf{c}$ is stable with respect to tilting, when $H_0 + K/M > 0$. Here K is the sum of the magnetostriction-renormalized constants of uniaxial magnetic anisotropy. As in Sec. 4, we shall consider only the magnetoelastic mechanism of excitation. It is convenient to solve the problem of transverse ultrasound generation in this geometry in cyclic variables, since the eigenmodes of the ferromagnet are $Q_\pm = Q_x \pm iQ_y$. The linearized system of initial equations (1)–(4) can be written as before in the form of Eqs. (15), if we set formally $H_0 = 0$ and use the following expressions for γ, χ, S, and ξ

$$\gamma = \gamma_{44}, \quad \chi = gM/(\omega_{sk} - \omega), \quad S = S_4, \quad \xi = \gamma_{44}^2 M^2 \chi / \rho_M S_4^2, \tag{43}$$

where $\omega_{sk} = \omega_0 + gM\alpha k^2$—is the eigenfrequency of nonuniform precession of the magnetization in the ferromagnet and S_4 is the velocity of transverse ultrasound propagating along the sixfold axis. Right- and left-polarized oscillations can be taken into account simultaneously in the system of equations (15), if formally we set in Eq. (43) $\omega > 0$ for right-polarized and $\omega < 0$ for left-polarized waves. Unlike the previous cases it is important for the analysis of the generation of transverse ultrasound that in Eqs. (15) the inhomogeneous exchange interaction is taken into account. The presence of the inhomogeneous exchange interaction leads to dispersion in the spectrum of spin waves and makes it necessary to consider the boundary conditions for the magnetization. Once again the dispersion equation of coupled oscillations can be written in the form (13), where it is necessary, however, to set the electromagnetic-acoustic conversion parameter ε equal to zero.

In the case of generation of transverse ultrasound in a normal magnetic field the general solution of system (15) for the waves propagating in the magnet can be written as

$$Q = \sum_{j=1}^{3} Q_j \exp(ik_j z), \tag{44}$$

where k_j are the roots of the dispersion equation (13).

The constants Q_j are determined from the boundary conditions, which in this case can be written as

$$\begin{gathered} h_0 + h_{Rx} + i\,\mathrm{sign}(\omega) h_{Ry} = \sum_{j=1}^{3} h_j, \\ -i\,\mathrm{sign}(\omega)(h_0 - h_{Rx}) + h_{Ry} = \frac{c\rho}{4\pi} \sum_{j=1}^{3} k_j h_j, \\ iC_{44} \sum_{j=1}^{3} k_j u_j + \gamma_{44} M \sum_{j=1}^{3} m_j = 0, \\ \sum_{j=1}^{3} k_j m_j = 0, \end{gathered} \tag{45}$$

where $\mathbf{h}_R$ is the wave reflected from the surface. The last of the conditions (45) corresponds to the absence of surface magnetic anisotropy (free spins).

The solution of the problem of electromagnetic generation of transverse ultrasound is the following expression for the displacement u ($u = u_+$ for $\omega > 0$, and $u = u_-$ for $\omega < 0$)

$$u = \frac{2i\gamma_{44} M h_0}{\rho_M \alpha S_4^2 R(k_1, k_2, k_3)} \{k_1 [k_2(k_A^2 - k_2^2) - k_3(k_A^2 - k_3^2)] \exp(ik_1 z) + \text{cyclic permutation}\}, \tag{46}$$

where

$$R(k_1, k_2, k_3) = \{[(k_A^2 - k_1^2)(k_M^2 - k_1^2) - k_A^2 k_{MA}^2] \times [k_2(k_A^2 - k_2^2) - k_3(k_A^2 - k_3^3)] + \text{cyclic permutation}\}. \tag{47}$$

Here $k_M^2 = (\omega - \omega_0)/gM\alpha$, $k_{MA}^2 = \xi/\alpha$.

In general, the expressions obtained are very complicated to analyze, hence it is convenient to do so for some limiting cases. It is known that in the geometry considered ($\mathbf{H}_0 \perp \mathbf{h}$) the ferromagnetic resonance $\omega = \omega_0$ takes place when the frequency of the ac magnetic field coincides with the frequency of uniform precession of magnetization.

Let us consider first the generation of transverse ultrasound at frequencies far from the ferromagnetic resonance. In this case the largest of the wavevectors under consideration is the spin wavevector $\mathbf{k}_M$. Approximate values of the roots of the dispersion equation (13) are

$$\begin{gathered} k_1^2 = \frac{\omega^2}{S_4^2} \times \begin{cases} \dfrac{\omega - \omega_{s0}}{\omega - \omega_0}, & \beta \gg 1, \\ \dfrac{\omega - \omega_{s0} - \omega_M}{\omega - \omega_0 - \omega_M}, & \beta \ll 1, \end{cases} \\ k_2^2 = \frac{2i}{\delta^2} \times \begin{cases} \dfrac{\omega - \omega_{s0} - \omega_M}{\omega - \omega_{s0}}, & \beta \gg 1, \\ \dfrac{\omega - \omega_0 - \omega_M}{\omega - \omega_0}, & \beta \ll 1, \end{cases} \\ k_3^2 = (\omega - \omega_0)/gM\alpha. \end{gathered} \tag{48}$$

Here k_1, k_2 and k_3 correspond to the quasielastic, quasielectromagnetic, and quasispin waves, respectively. In highly conducting materials the case of $\beta \gg 1$ is realized at frequencies $\omega > 10^{10}\ \mathrm{s}^{-1}$, while the case of $\beta \ll 1$ is realized at $\omega < 10^8\ \mathrm{s}^{-1}$.

The amplitude of the right-polarized transverse ultrasound u_+ in the most interesting frequency range ($\omega_0 < \omega < \omega_{s0}$ for $\beta \gg 1$ and $\omega_0 < \omega < \omega_0 + \omega_M$ for $\beta \ll 1$) is given by

$$u_+ = \frac{g\gamma_{44} M^2 h_0}{\rho_M S_4^3} \times \begin{cases} \dfrac{2\omega_{MA}\omega g M\alpha}{(\omega-\omega_0)^{5/2}(\omega_{s0}-\omega)^{1/2}}, & \beta \gg 1, \\ \delta^2 \omega \dfrac{(\omega_M+\omega_{s0}-\omega)^{1/2}}{(\omega_M+\omega_0-\omega)^{3/2}}, & \beta \ll 1. \end{cases} \tag{49}$$

In the frequency range $\omega < \omega_0 < \omega_{s0}$, $\omega_M + \omega_0$ the second formula in Eq. (49) remains unchanged, while the first should be written as

$$u_+ = \frac{2g\gamma_{44}M^2 h_0}{\rho_M S_4 \omega} \frac{1}{(\omega_0-\omega)^{1/2}(\omega_{s0}-\omega)^{1/2}}, \quad \beta \gg 1 \tag{50}$$

The amplitude of the left-polarized transverse ultrasound u_- in any frequency range can also be expressed by Eqs. (49) and (50). For $\beta \gg 1$ the amplitude u_- is determined by Eq. (50), while for $\beta \ll 1$ it is given by the second formula in Eq. (49) if ω is replaced by $-\omega$. Note, that for $\beta \gg 1$ and $\omega > \omega_0$ the right-polarized wave with wavenumber $k = k_3$ propagates in the magnet, while in other cases the propagating wave has wavenumber $k = k_1$. The left-polarized wave propagates always with wavenumber $k = k_1$. The oscillations with any other k are attenuated strongly near the metal surface.

Equations (49) and (50) thus show that in the case $\beta \gg 1$ the generation peaks up at the frequency of magnetoacoustic resonance $\omega = \omega_{s0} = \omega_0 + \omega_{MA}$ ($\omega_{MA} = g\gamma_{44}^2 M^3/\rho_M S_4^2$). In this case the oscillations of magnetization are not accompanied by excitations in elastic subsystem, a situation which corresponds to the concept of a "frozen lattice".[93] In the opposite case ($\beta \ll 1$) the amplitude of ultrasound increases at the frequency of magnetostatic resonance $\omega = \omega_0 + \omega_M$ ($\omega_M = 4\pi g M$), which corresponds to the concept of "free lattice".[93] Equations (49) and (50) can also be applied at the point of the spin-flip transition, where the frequency of uniform precession of the magnetization goes to zero. However, analyzing the electromagnetic-acoustic conversion one must take into account the dispersion of the spin waves. At the spin-flip frequency the amplitude of excited ultrasound increases also.

Consider now the generation of transverse ultrasound in the vicinity of the ferromagnet resonance. In this case the smallest of all the wavevectors is the spin wavevector $\mathbf{k}_M$. The roots of the dispersion equation (13) can be written as

$$k_{1,3}^2 = \pm \frac{\omega}{S_4}\left(\frac{\omega_{MA}}{gM\alpha}\right)^{1/2}, \quad k_2^2 = \frac{2i}{\delta^2}\left(1 + \frac{\omega_M}{\omega_{MA}}\right), \quad \beta \gg 1,$$
$$k_{2,3}^2 = \pm \frac{1+i}{\delta}\left(\frac{\omega_M}{gM\alpha}\right)^{1/2}, \quad k_1^2 = \frac{\omega^2}{S_4^2}\left(1 + \frac{\omega_{MA}}{\omega_M}\right), \quad \beta \ll 1. \tag{51}$$

The amplitude of excitation u_+ is expressed by

$$u_+ = \frac{\sqrt{2}g^{3/4}\gamma_{44}M^{7/4}h_0}{\rho_M \omega^{3/2}\omega_{MA}^{3/4}\alpha^{1/4}S_4^{1/2}}, \quad \beta \gg 1,$$
$$u_+ = \frac{g\gamma_{44}M^2 h_0 \omega \delta^2}{\rho_M S_4^3 \omega_M}(1 + \omega_{MA}/\omega_M)^{1/2}, \quad \beta \ll 1. \tag{52}$$

A comparison of Eqs. (49), (50), and (52) shows, that the amplitude of the transverse ultrasound generated increases substantially at the frequency of the ferromagnetic resonance.

The analysis carried out in this chapter allows us to formulate the approximations by which we can neglect the inhomogeneous exchange interaction in the expression for the free energy (9), and thus in the spectrum of quasispin waves and in the velocity of quasielastic oscillations. For $\beta \gg 1$ this approximation can be written as $\omega \ll \omega_0$, and for $\beta \ll 1$ as $\omega \ll \omega_0 + \omega_M$, which corresponds to frequencies far from either the ferromagnetic, or the magnetostatic resonances. In these approximations the second formula in Eq. (49) and Eq. (50) coincide with Eq. (23) and the EAC efficiency η is given by Eq. (24) if we use in the latter the expression $\chi = gM/\omega_{s0}$ for the susceptibility and $\xi = \omega_{MA}/\omega_{s0}$ for the magnetoelastic coupling parameter.

The electromagnetic excitation of transverse ultrasound in a magnetic field normal to the metal surface has been investigated experimentally for single-crystal nickel.[48-50,55,59,87] The field dependences of the conversion efficiency for various orientations of the static and ac magnetic fields with respect to the crystallographic axes of nickel are shown in Figs. 11 and 27. In all these cases the static magnetic field was oriented at some angle to the direction of spontaneous magnetization, thereby inducing a rotation of the magnetization to the direction of field $\mathbf{H}_0$. Comparing Figs. 12 and 27, one can see that the efficiency of excitation of transverse ultrasound increases at those magnetic fields when the efficiency of longitudinal ultrasound generation sharply decreases. These experimental results agree completely with Eqs. (35) and (49) for $\beta \ll 1$.

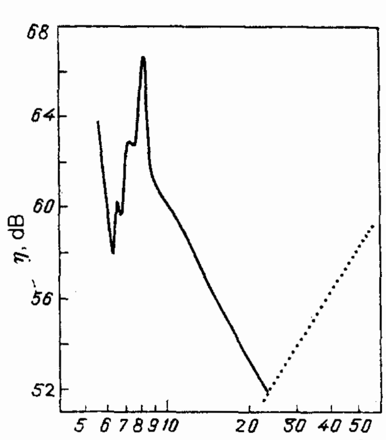

FIG. 27. Magnetic field dependence of the efficiency of transverse ultrasound excitation in single-crystal Ni at $\omega/2\pi = 15$ MHz, $T = 293$ K, $\mathbf{H}_0 \| \mathbf{q} \| [110]$, $\mathbf{h} \| [1\bar{1}0]$.[55]

CONCLUSIONS

As stated above, the conversion of electromagnetic and acoustic waves in conducting media is due to various physical interactions, i.e., inductive, deformational, inertial, thermoelastic, and magnetoelastic interactions. All of these interactions show up differently in various materials and under different experimental conditions. Even the simplest of them—the inductive mechanism—may change considerably if the normal and anomalous Hall effects in ferromagnets are taken into account [see Eq. (6)]. We have stressed the magnetoelastic interaction in ferromagnetic metals, and it has turned out that its manifestations in the electromagnetic excitation of ultrasound are quite diverse. In practice, every process that causes magnetization of a substance shows up, and sometimes in a very unexpected way, in the generation of ultrasound.

The analysis of the electromagnetic generation of ultrasound in ferromagnetic metals should be supplemented by the study of this phenomenon in metals with other types of magnetic ordering, as well as in ferroelectric insulators. This analysis, however, would substantially enlarge the scope of this paper, so we wish to consider only the main features of the electromagnetic-acoustic conversion processes in the magnets mentioned. Strictly, the study of EAC in magnetic insulators involving propagating elastic modes in magnetostrictors requires a special approach. These materials, conversely, are used for the generation of ultrasonic waves, since the conversion of electromagnetic and acoustic waves in them occurs over the entire volume. For the excitation of elastic waves in ferromagnets one can use the detector used in the study of EAC in semiconducting[94] and superconducting[95] materials. This device consists of a metal film with a thickness equal to the penetration depth of the metal deposited on the sample. Intense generation of ultrasound does not occur in general in antiferromagnetic metals in the region where magnetic ordering is established (the Neél point), but EAC can be observed as a result of spin flip.

The basic propositions of the theory of the magnetoelastic mechanism of electromagnetic-acoustic conversion have been illustrated in this paper with the example of the well studied 3d and 4f magnets. This approach is a natural one in the formulation of a new method of studying the magnetic and magnetoelastic characteristics of magnetically ordered media. However, even at this stage it has provided a more precise determination of a number of important parameters of these materials. For this analysis it can be seen that the quantitative results of the study of the electromagnetic acoustic conversion should be supplemented with measurements of the electrical, magnetic, and elastic properties of the materials. In carrying out this program it will be possible to determine the constants of the magnetic anisotropy, the homogeneous and inhomogeneous exchange interaction, and of the volume and relativistic magnetostriction and to determine the boundaries of the various magnetic states of magnets (the H_0–T diagram).

The authors anticipate that the phenomena of electromagnetic generation of ultrasound in magnetoordered materials can be used successfully to study the numerous newly synthesized compounds with various magnetic structures.

In conclusion the authors express their gratitude to M. I. Kaganov, A. V. Andrianov, Yu. P. Gaidukov, and V. G. Shavrov for a discussion of the results.

[1] V. M. Kontorovich and A. M. Glutsyuk, Zh. Eksp. Teor. Fiz. **41**, 1195 (1961) [Sov. Phys. JETP **14**, 852 (1961)].
[2] V. M. Kontorovich and N. A. Tishchenko, Izv. Vyssh. Uchebn. Zaved. Radiofiz. **6**, 24 (1963).
[3] V. M. Kontorovich, Zh. Eksp. Teor. Fiz. **59**, 2116 (1970) [Sov. Phys. JETP **32**, 1146 (1971)].
[4] M. I. Kaganov and V. B. Fiks, Fiz. Met. Metalloved. **19**, 489 (1965).
[5] M. I. Kaganov and V. B. Fiks, Fiz. Met. Metalloved. **26**, 11 (1968).
[6] M. I. Kaganov and V. B. Fiks, Zh. Eksp. Teor. Fiz. **62**, 1461 (1972) [Sov. Phys. JETP **35**, 767 (1972)].
[7] V. F. Gantmakher and V. T. Dolgopalov, Zh. Eksp. Teor. Fiz. **57**, 132 (1969) [Sov. Phys. JETP **30**, 76 (1970)].
[8] V. T. Dolgopolov, Zh. Eksp. Teor. Fiz. **61**, 1545 (1971) [Sov. Phys. JETP **34**, 823 (1971)].
[9] E. A. Kaner, V. L. Fal'ko, and L. P. Sal'nikova, Fiz. Nizk. Temp. **12**, 831 (1986) [Sov. J. Low Temp. Phys. **12**, 471 (1986)].
[10] E. A. Kaner and V. L. Falko, Solid State Commun. **35**, 353 (1980).
[11] M. R. Gaerttner, W. D. Wallace, and B. W. Maxfield, Phys. Rev. **184**, 702 (1969).
[12] D. E. Chimenti, C. A. Kukkonen, and B. W. Maxfield, Phys. Rev. B **10**, 3228 (1974).
[13] N. C. Banik and A. W. Overhauser, Phys. Rev. B **16**, 3379 (1977).
[14] N. C. Banik and A. W. Overhauser, Phys. Rev. B **18**, 3838 (1978).
[15] G. Laceuva and A. W. Overhauser, Phys. Rev. B. **30**, 5525 (1984).
[16] L. R. Ram Mohan, E. Kartheuser, and S. Rodriguez, Phys. Rev. B **20**, 3233 (1979).
[17] G. Feyder, E. Kartheuser, L. R. Ram Mohjan, and S. Rodriguez, Phys. Rev. B. **25**, 7141 (1982).
[18] G. Feyder, E. Kartheuser, L. R. Ram Mohjan, and S. Rodriguez, Phys. Rev. B **27**, 3213 (1983).
[19] G. Feyder, E. Kartheuser, L. R. Ram Mohjan, and S. Rodriguez, Phys. Rev. B **27**, 7107 (1983).
[20] S. Gopalan, G. Feyder, and S. Rodriguez, G. Phys. Rev. B **28**, 7323 (1984).
[21] E. Kartheuser and S. Rodriguez, Phys. Rev. B **33**, 772 (1986).
[22] S. Rodriguez, E. Kartheuser, and L. R. Ram Mohan, Adv. Phys. **35**, 423 (1986).
[23] Yu. P. Gaidukov and A. P. Perov, Pis'ma Zh. Eksp. Teor. Fiz. **8**, 666 (1968) [JETP Lett. **8**, 412 (1968)].
[24] Yu. P. Gaidukov and A. P. Perov, Pis'ma Zh. Eksp. Teor. Fiz. **9**, 585 (1969) [JETP Lett. **9**, 356 (1969)].
[25] Yu. P. Gaidukov and A. P. Perov, Akust. Zh. **17**, 314 (1971) [Sov. Phys. Acoust. **17**, 266 (1971)].
[26] V. Ya. Kravchenko Zh. Eksp. Teor. Fiz. **54**, 1494 (1968) [Sov. Phys. JETP **27**, 801 (1968)].
[27] K. B. Vlasov, V. G. Kuleev, and E. V. Rozenfel'd, Fiz. Met. Metalloved. **35**, 5 (1973).
[28] K. B. Vlasov and V. G. Kuleev, Fiz. Met. Metalloved. **25**, 15 (1968).
[29] K. B. Vlasov and V. G. Kuleev, Fiz. Tverd. Tela (Leningrad) **9**, 3022 (1967) [Sov. Phys. Solid State **9**, 2386 (1967)].
[30] J. J. Quinn, Phys. Lett. A, **25**, 522 (1967).
[31] J. J. Quinn, J. Phys. Chem. Solids **31**, 1701 (1970).
[32] J. J. Quinn, Phys. Rev. Lett. **24**, 817 (1970).
[33] R. C. Alig, Phys. Rev. **178**, 1050 (1969).
[34] P. D. Southgate, J. Appl. Phys. **40**, 22 (1969).
[35] A. G. Betjemann, H. V. Bohm, D. J. Meredith, and E. R. Dobbs, Phys. Lett. A **25**, 753 (1967).
[36] D. J. Meredith, R. J. Watts-Tobin, and E. R. Dobbs, J. Acoust. Soc. Amer. **45**, 1393 (1968).
[37] E. R. Dobbs, R. L. Thomas, and D. Hsu, Phys. Lett. A **30**, 338 (1969).
[38] E. R. Dobbs, J. Phys. Chem. Solids **31**, 1657 (1970).
[39] W. D. Wallace, Int. J. Nondestr. Test. **2**, 309 (1971).
[40] E. R. Dobbs, *Physical Acoustics*, Academic, New York (1973), Vol. 10, p. 127.
[41] A. N. Vasiliev and Yu. P. Gaidukov, Usp. Fiz. Nauk **141**, 431 (1983) [Sov. Phys. Usp. **26**, 952 (1983)].
[42] M. I. Kaganov, Zh. Eksp. Teor. Fiz. **98**, 1828 (1990) [Sov. Phys. JETP **71**, 1028 (1990)].
[43] V. L. Gurevich, I. G. Lang, and S. T. Pavlov, Zh. Eksp. Teor. Fiz. **59**, 1679 (1970) [Sov. Phys. JETP **32**, 914 (1970)].
[44] K. P. Belov, *Magnetostriction Phenomena and Their Technological Application* [in Russian], Nauka, Moscow (1987).
[45] G. A. Budenkov, S. Yu. Gurvich, and A. F. Maskaev, *Physical Methods of Testing Materials* [in Russian], Ural Polytechnic Institute, Chelyabinsk (1980), p. 11.
[46] G. A. Buydenkov and A. F. Maskaev, Defektoskopiya No. 5, 83 (1972).
[47] G. A. Budenkov and A. F. Maskaev, Defektoskopiya No. 1, 109 (1973).
[48] M. B. Gimis, Fiz. Tverd. Tela (Leningrad) **14**, 3563 (1972) [Sov. Phys. Solid State **14**, 2992 (1972)].
[49] V. F. Drobot'ko and V. P. Naberezhnykh, Fiz. Nizk. Temp. **2**, 872 (1976) [Sov. J. Low Temp. Phys. **2**, 428 (1976)].

[50] V. F. Drobot'ko and V. P. Naberezhnykh, Fiz. Nizk. Temp. **6**, 72 (1980) [Sov. J. Low Temp. Phys. **6**, 35 (1978)].
[51] R. S. Il'yasov and V. A. Komarov, Defectoskopiya No. 12, 34 (1982).
[52] R. S. Il'yasov and V. A. Komarov, Defectoskopiya No. 11, 53 (1983).
[53] M. J. W. Povey, E. R. Dobbs and D. J. Meredith, J. Phys. F **3**, L234 (1973).
[54] M. J. W. Povey, E. R. Dobbs and D. J. Meredith, J. Phys. F **10**, 2555 (1980).
[55] M. J. W. Povey, D. J. Meredith, and E. R. Dobbs, J. Phys. F **10**, 2041 (1980).
[56] I. A. Privorotskii, A. B. Devine, and G. C. Alexandrakis, J. Appl. Phys. **50**, 7732 (1979).
[57] G. C. Alexandrakis and A. B. Devine, Solid State Commun. **41**, 781 (1982).
[58] R. A. Gordon, J. Appl. Phys. **52**, 4729 (1979).
[59] M. Hanabusa, T. Kushida, and J. C. Murphy, J. Appl. Phys. **44**, 5106 (1973).
[60] G. Gorodetsky, B. Luthi, T. J. Moran, and M. E. Mullen, J. Appl. Phys. **43**, 1234 (1972).
[61] A. V. Andrianov, A. N. Vasil'ev, Yu. P. Gaidukov, and R. S. Il'yasov, Fiz. Met. Metalloved. **64**, 1036 (1987).
[62] A. V. Andrianov, A. N. Vasil'ev, Yu. P. Gaidukov, and R. S. Il'yasov, Fiz. Met. Metalloved. **67**, 708 (1989).
[63] A. V. Adrianov, A. N. Vasil'ev, Yu. P. Gaidukov, and R. S. Il'yasov, Pis'ma Zh. Eksp. Teor. Fiz. **45**, 571 (1987) [JETP Lett. **45**, 729 (1987)].
[64] A. V. Andrianov, V. D. Buchel'nikov, A. N. Vasil'ev *et al.*, Zh. Eksp. Teor. Fiz. **94**(11) 277 (1988) [Sov. Phys. JETP **67**, 2331 (1988)].
[65] A. V. Andrianov, A. N. Vasil'ev, Yu. P. Gaidukov *et al.*, Pis'ma Zh. Eksp. Teor. Fiz. **49**, 621 (1989) [JETP Lett. **49**, 715 (1989)].
[66] A. V. Adrianov, V. D. Buchel'nikov, A. N. Vasil'ev *et al.*, Zh. Eksp. Teor. Fiz. **97**, 1674 (1990) [Sov. Phys. JETP **70**, 944 (1990)].
[67] A. V. Andrianov, Yu. P. Gaidukov, A. N. Vasil'ev, and E. Fawcett, J. Magn. Magn. Mater. **97**, 246 (1991).
[68] R. B. Thompson, IEEE Ultrasonics Symposium Proc. (1976), p. 585.
[69] R. B. Thompson, IEEE Ultrasonics Symposium Proc. (1976), p. 74.
[70] R. B. Thompson, IEEE Trans. Sonics Ultrason. **TSU-25**, 7 (1978).
[71] H. M. Frost, Phyical Acoustics, **14**, 179, Academic, New York (1979).
[72] G. A. Budenkov, S. Yu. Gurevich, and A. F. Maskaev, Defectoscopiya No. 5, 5 (1981).
[73] Yu. M. Shkarlet, *Contactless Methods of Ultrasonic Testing* [in Russian], Mashinostroenie, Moscow (1974).
[74] V. A. Komarov, *Quasi-Stationary Electromagnetic-Acoustic Conversion in Metals* [in Russian], Ural Scientific Center, Academy of Sciences of the USSR, Sverdlovsk.
[75] V. G. Baryakhtar, A. M. Grishin, and V. F. Drobot'ko, Fiz. Nizk. Temp. **7**, 1486 (1981) [Sov. J. Low Temp. Phys. **7**, 720 (1981)].
[76] A. I. Akhiezer, V. G. Bar'yakhtar, and S. V. Peletminskii, *Spin Waves* [in Russian], Nauka, Moscow (1967).
[77] K. P. Belov, A. K. Zvezdin, A. M. Kadometseva, and R. Z. Levitin, *Orientational Transitions in Rare-Earth Magnets* [in Russian], Nauka, Moscow (1979).
[78] R. A. Alpher and R. J. Rubin, J. Acoust. Soc. Am. **26**, 452 (1954).
[79] A. N. Vasil'ev and Yu. P. Gaidukov, Zh. Eksp. Teor. Fiz. **81**, 2234 (1981) [Sov. Phys. JETP **54**, 1186 (1981)].
[80] A. N. Vasil'ev, Yu. P. Gaidukov, M. I. Kaganov *et al.*, Fiz. Nizk. Temp. **15**, 160 (1989) [Sov. J. Low Temp. Phys. **15**, 91 (1989)].
[81] G. J. Parkinson and D. W. Wilson, Brit. J. Nondestr. Test. **7**, 178 (1977).
[82] E. A. Tyurov and A. A. Lugovio, Fiz. Met. Metalloved. **50**, 903 (1980).
[83] A. G. Gurevich, *Magnetic Resonance in Ferrites and Antiferromagnets* [in Russian], Nauka, Moscow (1973).
[84] K. P. Belov, M. A. Belyhanchikova, R. Z. Levitin, and S. A. Nikitin, *Rare-Earth Ferromagnets and Antiferromagnets* [in Russian], Nauka, Moscow (1965).
[85] Yu. I. Sirotin and M. P. Shaskol'skaya, *Fundamentals of Crystallography* [in Russian], Nauka, Moscow (1979).
[86] A. N. Vasil'ev, V. V. Kokorin, Yu. I. Savchenko *et al.*, Zh. Eksp. Teor. Fiz. **98**, 1437 (1990) [Sov. Phys. JETP **71**, 803 (1990)].
[87] E. A. Pacher and B. W. Maxfield, IEEE Ultrasonics Symp. Proc. (1974), p. 526.
[88] R. Herz and H. Kronmuller, J. Magn. Magn. Mater. **9**, 273 (1978).
[89] M. Akhavan, H. A. Blackstead, and P. L. Donoho, Phys. Rev. B **8**, 4258 (1973).
[90] C. Isci and S. B. Palmer, J. Phys. F **8**, 247 (1978).
[91] U. Enz, Physica **26**, 698 (1960).
[92] D. J. Martin and J. J. Rhune, J. Phys. C. **10**, 4123 (1977).
[93] E. A. Turov and V. G. Shavrov, Usp. Fiz. Nauk **140**, 429 (1983) [Sov. Phys. Usp. **26**, 573 (1983)].
[94] A. N. Vasil'ev, V. N. Nikiforov, I. M. Malinski *et al.*, Semicond. Sci. Technol. **5**, 1105 (1990).
[95] V. Muler, C. Hucho, and D. Maurer, *Ferroelectrics* (1992).

Translated by the Authors

Note from the Translation Editor: This paper has been edited in order to conform to the Russian text.